國 立 交 通 大 學
光 電 工 程 研 究 所

碩士論文

氮化鎵奈米柱製程與雷射特性之研究

Fabrication and lasing characteristics of GaN nanopillars

研究生：何依寧

指導教授：郭浩中 教授

盧廷昌 教授

中 華 民 國 九 十 九 年 七 月

氮化鎵奈米柱製程與雷射特性之研究

Fabrication and lasing characteristics of GaN nanopillars

研究生:何依寧 Student: Yi-Ning He

指導教授:郭浩中 教授 Advisor: Prof. Hao-Chung Kuo

盧廷昌 教授 Prof. Tien-Chang Lu

國 立 交 通 大 學

光電工程研究所

碩 士 論 文

A Thesis

Submitted to Institute of Electro-Optical Engineering

College of Electrical Engineering

National Chiao Tung University

in Partial Fulfillment of the Requirements

for the Degree of

Master

In

Electro-Optical Engineering

June 2009

Hsinchu, Taiwan, Republic of China

氮化鎵奈米柱製程與雷射特性之研究

研究生：何依寧　　　　　　　　　　指導教授：郭浩中教授

盧廷昌教授

國立交通大學光電工程研究所碩士班

摘要

本論文中，我們利用快速熱退火(rapid thermal annealing, RTA) 將鎳聚成奈米小球，再使用電漿離子耦合反應系統(ICP-RIE)將氮化鎵蝕刻成柱狀，將小球洗掉後，成長一層氮化鎵在奈米柱的表面。我們使用刀鋒量測來得知雷射光點大小，以便估算雷射能量密度。在特性分析中，包含了結構與光學特性上的相關研究。在發光特性方面，所利用的是脈衝光激發螢光光譜((Microphotoluminescence, μ-PL)，以及變角度和低溫光譜等進行樣品的光學與電特性分析。

藉由變功率脈衝雷射激發去探討室溫時氮化鎵奈米柱的雷射特性，比起未包覆一層氮化鎵的奈米柱，會有更低的閾值功率密度，和較高的自發放射因子(β value)。氮化鎵奈米柱的雷射波長會隨著光點範圍增大而有所紅移，且閾值功率密度和模態間距隨之下降。變角度實驗結果顯示做成奈米柱後，重新包覆過後的斜面結構使樣品的出光散射現象，存在方向性(10°, -15°)。另外由低溫量測中，我們可以得知奈米柱的特徵溫度約 153K。由於氮化鎵雷射具有許多優越的光學特性，我們相信此結構可以應用在可見光及藍紫光雷射等高功率、大範圍及多用途之光電元件中。

Fabrication and lasing characteristics of GaN nanopillars

Student : Yi-Ning He Advisor: Prof. Hao-Chung Kuo

Prof. Tien-Chang Lu

Institute of Electro-Optical Engineering

National Chiao Tung University

Abstract

In this study, we studied GaN nanopillars structure fabricated by combined two methods top-approch and bottom-approch. The sample of GaN nanopillars etched down by ICP-RIE with Ni nano mask ,then regrowth GaN passivation layer in the sidewalls. The spotsize dependent photoluminescence (PL), and angle-resolved PL and low temperature were performed to investigate the optical properties of the GaN nanopillars.

This research intends to investigate the lasing characteristics of GaN nanopillars under optical pumping. GaN nanopillars has lower threshold power density and higher β value than etched pillars without passivation. The spotsize dependence of the lasing PL spectrum has been observed. As excitation spotsize increasing, the central position of lasing peak wavelength was gradual red-shift, threshold power density decreased and the number of lasing multi-peak modes dreased. We suggest that the

peak shift effect of lasing peak was attributed to the change of material gain spectrum under different pumping condition, not related to the pumping power intensity under change of spot size. The angle-resolved PL results show the degree of emission anlges corresponding to the normal direction (10˚, -15˚) respectively.

Moreover, it was observed that the increase in temperature (from 77K to 322K) leads to an increase in threshold excitation energy. It is due to the increase of non-radiated recombination and decrease of radiated recombination. The characteristic temperature T_0, was estimated to be 153 K in the temperature range of 77K to 322K.

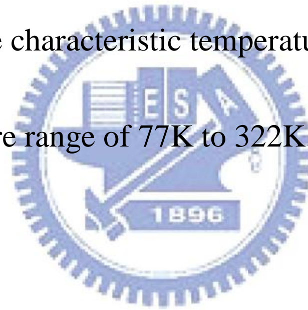

誌謝

在這兩年的研究生活中，首先感謝指導教授郭浩中老師、盧廷昌老師、王興宗老師和中研院的程育人老師。在我研究的領域上遭遇困難時，提供很多的意見以及幫助，讓實驗更為順利。感謝明華學長在實驗上的帶領，不厭其煩的教導我儀器及實作上的學問，常常會生出很多好吃的水果給大家吃，還總是在緊急關頭跳出來救我，真的很罩。

感謝我的好姐妹，惟雯、小邱和玫君，陪我一起敗家，一起聊女人話題，一起講些狗屁倒灶的事，有妳們真好，希望妳們接下來都可以幸福。感謝又帥又陽光的小三八，請不要辜負我對你身為第六姬電子淇的期望。感謝獸皇大大，你真的是個好揪又好嗆的咖，平時麻煩你很多，請不要說我壞話。感謝喵喵警長David，祝你可以住在深海的大鳳梨裡，擁有一條掉不下來的褲子。感謝念女校的阿伯，祝你早日找到白馬王子。感謝火星人永吉，會很有耐心的回答我稀奇古怪的問題。感謝彈耳朵很痛的小昕，你是女生公認溫柔派第一名。感謝很不受控制的嗡嗡，每次有你在的地方就會high到不行。感謝很白爛的阿菲，辦事很有效率又條理分明。感謝又高又帥的阿祥，你打球超厲害的。感謝眼睛很迷濛的哭哭，感謝慢條斯理的小胖，感謝你們以上這些臭男生，害我聽黃色笑話和打電動的功力越來越高。感謝俊榮學長，碩一的時候常受你照顧，祝你工作順利萬萬歲。感謝小柯，不管是在實驗或生活玩樂上，還是常給我中肯的建議。

謝謝所有的學長姐學弟妹們，謝謝大家陪我度過精采的兩年碩班生活，我會很想很想你們的。謝謝我的家人，默默的支持我，包容我的任性，讓我順利完成學業。

Content

摘要……………………………………………………………………………i
Abstract..ii
致謝……………………………………………………………………………..iv
Content..v
List of Tables..vii
List of Figures..viii

Chapter 1 Introduction

1.1 Development of III-nitrides materials…………………………………….....1

1.2 Characteristic of Gallium Nitride……………………………….……...2

1.3 Reference……………………………..……………………………...6

Chapter 2 Motivation of GaN nanostructure

2.1 Fabrication of nanostructure materials……………………………………...8

2.2 Methods of fabrication

2.2.1 Chemical-beam epitaxy of GaN nanorods………………………………10

2.2.2 Focused ion beam etching……………………………………………11

2.2.3 Inductively coupled plasma reactive ion etching (ICP-RIE) ………13

2.3 Motivation…………………………………………………………16

2.4 Reference……………...……………………………………………21

Chapter 3 Experimental principles and systems

3.1 Gaussian beams……………………..……………………………………27

3.2 Knife Edge………………………………………………………..............28

3.3 Microphotoluminescence spectroscopy(μ-PL) ……………………….......31

3.4 Pumping power density and spotsize calculation..…………………………..…32

3.5 Scanning electron microscope (SEM) …………………………………………35

3.6 Transmission electron microscope (TEM) ……………………………36

3.7 Charge coupled device (CCD) camera……….………………………………..37

3.8 Reference……………………………………………………………………43

Chapter 4 Fabrication and Characteristics of Optical Pumped Nitride-Based nanopillars

4.1 Fabrication of hexagonal GaN nanopillars……………………………………45

4.2 Characteristics of Optically Pumped Nitride-Based nanopillars

4.2.1 Optical pumping of GaN nanopillars at room temperautre………………...47

4.2.2 Lasing characteristics under different pump spotsize……………………49

4.2.3 Angle resolved PL………………………………………………………51

4.3 Temperature dependent threshold and characteristics temperature………………53

4.4 Reference……………………………………………………………………55

Chapter 5 Conclusion……………………………………………………..67

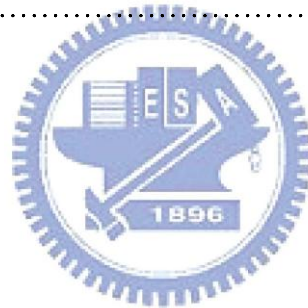

List of Tables

Table 3.4.1 Comparison of calculation results and experimental results…......40

List of Figures

Fig.1.2.1 Wurtzite crystal structure of Gallium Nitirde…………………………...5

Fig.2.1.1 Dimension of nanostructure and corresponding density of state……….19

Fig.2.2.2.1 The principle of FIB……………………………………………….…....19

Fig.2.2.3.1 A common RIE setup consists of two electrodes (1 and 4) that create an electric field (3) meant to accelerate ions (2) toward the surface of the samples (5)……………………………………………………..…....20

Fig.3.1.1 Gaussian beam…………………………………………….….…...39

Fig.3.2.1 Schematic of a scanning knife edge……………………………..…...39

Fig.3.2.2 Spot profile and measured signal…………………………….……....40

Fig 3.3.1 Nd:YVO4 355-nm pulsed laser microPL measurement system………..40

Fig.3.4.1. (a) Knife Edge measurement diagram (b) the distance between lens and knife is 2 5μm,and laser beam spotsize is about 4.6μm……….….…41

Fig.3.4.2. Laser spotsize calculation and experimental results by knife edge measurement……………………………………………….….………...41

Fig.3.5.1 Schematic diagram of a scanning electron microscope ……..……..…42

Fig.3.6.1 Ray diagram showing two basic operations of TEM(a) imaging p rojecting a diffraction pattern and (b) projection of an image onto a viewing screen………………………..…………………………...…42

Fig.4.1.1 Processing steps of nanopillars……………………..………………..58

Fig.4.1.2 (a)Ni-mask on Plane view (a), titled (b) and crossection (c) SEM image……………………………………..……………………..……..58

Fig 4.2.1.1 Power dependent PL spectrum of nanopillars with spotsize~13.5μm, and the stimulated emission wavelength at 369 nm……….………….59

Fig.4.2.1.2 Light intensity and FWHM versus excitation power density of pillars…………………………………………….…..……………..59

Fig.4.2.1.3 Power density dependent nanopillar and nanopillars without passivation (Ref) with spotsize~ 37.1μm ……………………...……60

Fig 4.2.1.4 Light intensity and FWHM versus excitation power density of pillar,Ref and bulk under 37.1μm laser beam………………………..…………60

Fig 4.2.1.5 Input-output characteristic on logarithmic scales. Solid symbols are experimental data, and the line is theoretical fitting……………………61

Fig 4.2.2.1 Power density dependent PL spectrum of pillar with various Spotsize…………………………………………………………..…..61

Fig 4.2.2.2 Threshold pumping power density of pillar with various spotsize……..62

Fig 4.2.2.3 Comparison of various spotsize PL spectra……………………...…..62

Fig 4.2.2.4 Emission wavelength and Threshold power density versus excitation spotsize of pillars……………………………………………..……63

Fig 4.2.2.5 Mode spacingof pillar under various spotsize …………………….……63

Fig 4.2.2.6 (a) GaN bulk gain spectra v.s spot size (b) Nanopillar gain spectra v.s spot size…………………………………………………………………..64

Fig 4.2.3.1 Angle-resolved μ-PL measurement system……………………….…..64

Fig 4.2.3.2 Angle-resolved μ-PL spectrum and intensity versus angle (a)GaN bulk (b) Nanopillars………………………………………...…65

Fig 4.3.1 Temperature dependent PL spectrum of pillar……………………..…65

Fig 4.3.2 The emission intensity-excitation energy curve at 77K, 252K,and 322K…………………………………………………………………...66

Fig 4.3.3 The temperature dependent threshold excitation power…………...….66

Chapter 1 Introduction

1.1 Development of III-nitrides materials

In recent decades, the III-nitrides InN, GaN, and AlN related alloys become an interesting class of wide bandgap materials and play an important role in semiconductor devices [1-7], especially for optoelectronics [1-3] as well as electronics. Since the wurtzite polytypes of III-nitrides form a continuous alloy system whose direct bandgap ranging from 0.7 eV for InN [8], to 3.4 eV for GaN, and to 6.2 eV for AlN [9], the optical devices using III-nitrides could be activated at wavelength ranging from red, green, blue, to deep ultraviolet. This phenomenon is quite different from other III-V materials systems based on GaAs, AlAs, InAs, GaP and related alloys. In addition, III-nitride material is the most promising material for ultraviolet light emitting sources.

GaN is a semiconductor compound used for blue, UV, and white (color mixing) LEDs; it allows high output power with small physical volume. The use of GaN has made possible applications, such as daylight visible full color LED displays, white LEDs and blue laser devices. The GaN LEDs typically comprise two thin layers of gallium nitride grown on sapphire or silicon carbide (SiC) substrates. GaN-based LEDs

(light-emitting diodes) are semiconductor devices that emit visible light when electricity is passed through them. Generally, the emitted light is monochromatic and the main benefits of this technology include: low power requirement; high efficiency; and long life. GaN LEDs are mainly used in the manufacturing of displays, signs, traffic signals, automotive lightning, domestic lightning, and medical sensors.

Pulsed oscillation of GaN semiconductor laser (LD) was reported in 1995 and continuous oscillation was reported in 1996. In 1999, 5mW LD was commercialized for the first time in the world. The application field of LD can be classified into the optical storage field and the industrial field, and in the field of optical storage, the large-capacity optical disk standard was announced in 2002, and future expansion of the market is expected.

1.2 Characteristics of Gallium Nitride

In materials science, GaN is often called a III-V semiconductor because Gallium and Nitride belong to the 3rd and 5th groups of the periodic table, respectively. GaN is a binary III-V direct bandgap semiconductor commonly used in bright light-emitting diodes since the

1990s. The compound is a very hard material that has a Wurtzite crystal structure. Its wide band gap of 3.4 eV affords it special properties for applications in optoelectronic, high-power and high-frequency devices. For example, GaN is the substrate which makes violet (405 nm) laser diodes possible, without use of nonlinear optical frequency-doubling. Its sensitivity to ionizing radiation is low (like other group III nitrides), making it a suitable material for solar cell arrays for satellites. Because GaN transistors can operate at much hotter temperatures and work at much higher voltages than gallium arsenide (GaAs) transistors, they make ideal power amplifiers at microwave frequencies.

GaN is a very hard, mechanically stable material with large heat capacity. In its pure form it resists cracking and can be deposited in thin film on sapphire or silicon carbide, despite the mismatch in their lattice constants. GaN can be doped with silicon (Si) or with oxygen to N-type and with magnesium (Mg) to p-type; however, the Si and Mg atoms change the way the GaN crystals grow, introducing tensile stresses and making them brittle. Gallium nitride compounds also tend to have a high spatial defect frequency, on the order of a hundred million to ten billion defects per square centimeter. GaN-based parts are very sensitive to

electrostatic discharge.

High crystalline quality GaN can be obtained by low temperature deposited buffer layer technology. This high crystalline quality GaN led to the discovery of p-type GaN, p-n junction blue/UV-LED and room-temperature stimulated emission (indispensable for laser action). This has led to the commercialization of high-performance blue LEDs and long-lifetime violet-laser diodes, and to the development of nitride-based devices such as UV detectors and high-speed field-effect transistors.

However, GaN and its heterostructure materials are usually epitaxial grown on a foreign substrate, such as sapphire, silicon, or silicon carbide because a large-size commercial grade native substrate is still not available at a low cost. A high

density of threading dislocation (TD) is therefore generated in the materials as a result of large lattice and thermal expansion coefficient mismatches between the GaN films and these substrates.[11]

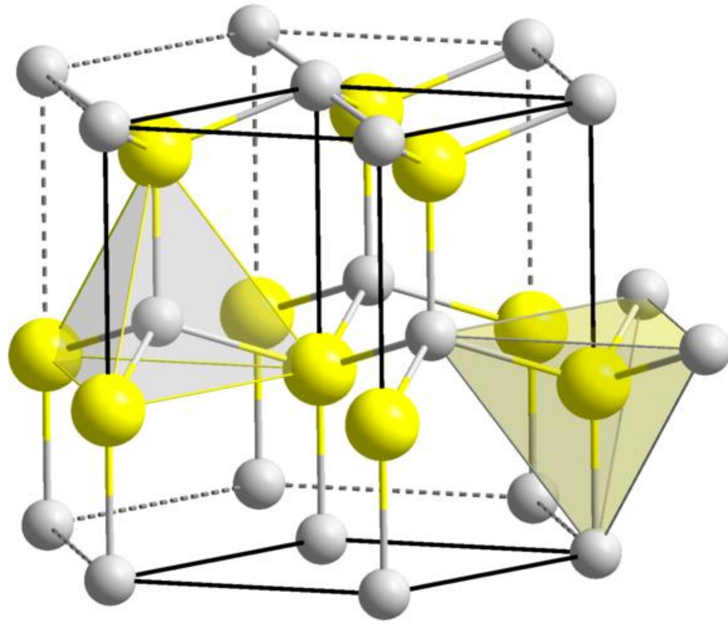

Fig 1.2.1 Wurtzite crystal structure of Gallium Nitirde

1.3 Reference

[1] S. Nakamura, T. Mukai, and M. Senoh, Appl. Phys. Lett., 67, 1687 (1994)

[2] S. Nakamura, M. Senoh, N. Iwasa, and S. Nagahama, Jpn. J. Appl. Phys., 34, L797 (1995)

[3] G. Y. Xu, A. Salvador, W. Kim, Z. Fan, C. Lu, H. Tang, H. Markoc, G. Smith, M. Estes, B. Goldberg, W. Yank, and S. Krishnankutty, Appl. Phys. Lett., 71, 2154 (1997)

[4] T. G. Zhu, D. J. H. Lambert, B. S. Shelton, M. N. Wong, U. Chowdhury, H. K. Kwon, and R. D. Dupuis, Electron Lett., 36, 1971 (2000)

[5] G. T. Dang, A. P. Zhang, F. Ren, X. A. Cao, S. J. Pearton, H. Cho, J. Han, J. I. Chyi, C. M. Lee, C. C. Chuo, S. N. G. Chu, and R. G. Wilson, IEEE Trans. Electron Devices, 47, 692 (2000)

[6] B. S. Shelton, D. J. H. Lambert, H. J. Jang, M. M. Wong, U. Chowdhury, Z. T. Gang, H. K. Kwon, Z. Liliental-Weber, M. Benarama, M. Feng, and R. D. Dupuis, IEEE Trans. Electron Devices, 48, 490 (2001)

[7] A. P. Zhang, J. Han, F. Ren, K. E. Waldrio, C. R. Abernathy, B. Luo, G. Dang, J. W. Johnson, K. P. Lee, and S. J. Pearton, Electronchem.

Solid-State Lett., 4, G39 (2001)

[8] T. Matsuoka, H. Okamoto, M. Nakao, H. Harima, and E. Kurimoto, Appl. Phys. Lett., 81, 1246 (2002)

[9] H. Morkoc, Nitride Semiconductors and devices, (Springer-Verlag, Berlin, 1999)

[10] C.-H. Lee, J. Yoo, Y. J. Hong, J. Cho, Y.-J. Kim, S.-R. Jeon, J. H. Baek, and

G.-C. Yi ”GaN/ In1−xGaxN/GaN/ZnO nanoarchitecture light emitting diode

microarrays, ” Appl. Phys. Lett. **94**, 213101. (2009)

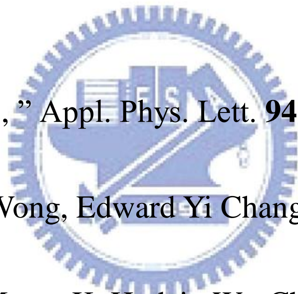

[11] Yuen-Yee Wong, Edward Yi Chang, Tsung-Hsi Yang, Jet-Rung Chang,Jui-Tai Ku, Mantu K. Hudait, Wu-Ching Chou, Micheal Chen, and Kung-Liang Lina “The Roles of Threading Dislocations on Electrical Properties of AlGaN/GaN Heterostructure Grown by MBE” Journal of The Electrochemical Society, **157**, 7 (2010)

Chapter 2 Motivaiton of GaN nanostructure

In this chapter, we show the different fabrication methods (CBE,FIB,ICP-RIE) about GaN nano structures and motivation of using ICP-RIE for our sample,GaN nanopillars.

2.1 Fabrication of nanostructure materials

Low dimension structure as the active layer was widely applied in these optical devices to operate in low threshold current, reduce temperature sensitivity and enhance the emitting efficiency due to quantum confine effect [1-2]. Because of the different dimensional confinement of carrier and density of state, the nanostructure can be classify into quantum well (QW), nanowire and quantum dot (QD) by their density of state as shown in Fig. 2.1.1. The bulk material has three dimensional density of state and the shape is parabolic function, the energy state of carrier is continues above energy band-gap. Then two dimensional structures, such as quantum well, is a step function due to one dimensional confinement of carrier. With decreasing the degree of freedom of carriers, the density of state of zero-dimensional structure, as quantum dot, manifest delta function density of state. As a result, the electronic states are quantized and the energy levels become discrete.

The fabrication of semiconductor nanostructures through patterning of planar layers is a well known technique. Using this top-down approach, well-ordered nanostripe and nano-pillar compound semiconductor arrays have been demonstrated.[3] The nanofeatures were either directly etched using a focused ion beam (FIB) or created through a combination of lithography and large area etching procedures such as reactive ion beam, inductively coupled plasma (ICP), or wet chemical etching. In addition to electron beam lithography,[4] In the past years other nanopatterning techniques were developed, for example, nanoimprinting,[5] the use of nonporous asking materials,[6] or self-assembled masks.[7]

The majority of investigations were directed towards bottom-up growth of group-III nitride nanowires or nanocolumns, using techniques such as catalyst assisted,[8–10] catalyst-free.growth,[11-14] or selective area deposition.[15-16]

Fewer studies were conducted to explore group-III nitride Fewer studies were conducted to explore group-III nitride nanostructure fabrication through etching,[17-19] although bright luminescence was observed from etched GaN and InGaN/GaN nanorod arrays.[20-22]

Interestingly, nonradiative recombination at free surfaces of GaN and

its alloys was seen to be significantly less pronounced than for (Al,Ga,In)(As,P) semiconductors.[23] Experiments also indicated that group-III nitrides are less susceptible to sidewall damage.[24] Etched nanorod arrays are, in particular, of interest for optoelectronic devices as, similar to micron-sized array LEDs, increased light extraction is expected from nanowires and nanorods over planar structures due to a higher surface area and reduced absorption.[25-27] Moreover, the light extraction can be further engineered using photonic crystal concepts.[28]

2.2 Methods of fabrication

2.2.1 Chemical-beam epitaxy of GaN nanorods

The chemical-beam epitaxy can be work in high vacuum circumstances at high temperature with low fabrication cost. Three-axle z-axis manipulator provides stable rotation capability and flexible expansibility. The design of heat module is able to work at high temperature up to 1100°C without harming the surrounding components. Group-V source is supplied by nitrogen plasma, which is beneficial for indium nitride growth. Group-III metalorganic sources are introduced into the growth chamber by a special designed gas source ring, which makes

the reactants hinge on the substrate surface efficiently and uniformly. The growth of dislocation free GaN nanorods on c-sapphire substrates by a CBE technique is demonstrated. By compared the CBE method with other common growth methods, the CBE is a more feasible technique to fabricate high-quality, high-density, and vertical-alignment GaN nanorods. Without extra metal catalyst required, the thickness and length distributions of each GaN nanorods were formed identically. Furthermore, the nanorods were grown epitaxially and were elongated in the direction parallel to the surface normal.

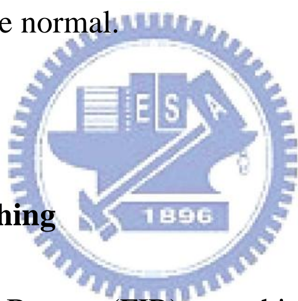

2.2.2 Focused Ion Beam Etching

Focused Ion Beam (FIB) machine is an excellent tool to semiconductor engineering analysis, using for the nano-fabrication of GaN. There are some advantage of FIB such as Direct Write , Maskless and Rapidly Process.[29]

Focused ion beam (FIB) systems have been produced commercially for approximately twenty years, primarily for large semiconductor manufacturers. FIB systems operate in a similar fashion to a scanning electron microscope (SEM) except, rather than a beam of electrons and as

the name implies, FIB systems use a finely focused beam of ions (usually gallium) that can be operated at low beam currents for imaging or high beam currents for site specific sputtering or milling.

As Fig 2.2.2.1, the gallium (Ga+) primary ion beam hits the sample surface and sputters a small amount of material, which leaves the surface as either secondary ions (i+ or i-) or neutral atoms (n^0). The primary beam also produces secondary electrons (e^-). As the primary beam rasters on the sample surface, the signal from the sputtered ions or secondary electrons is collected to form an image.

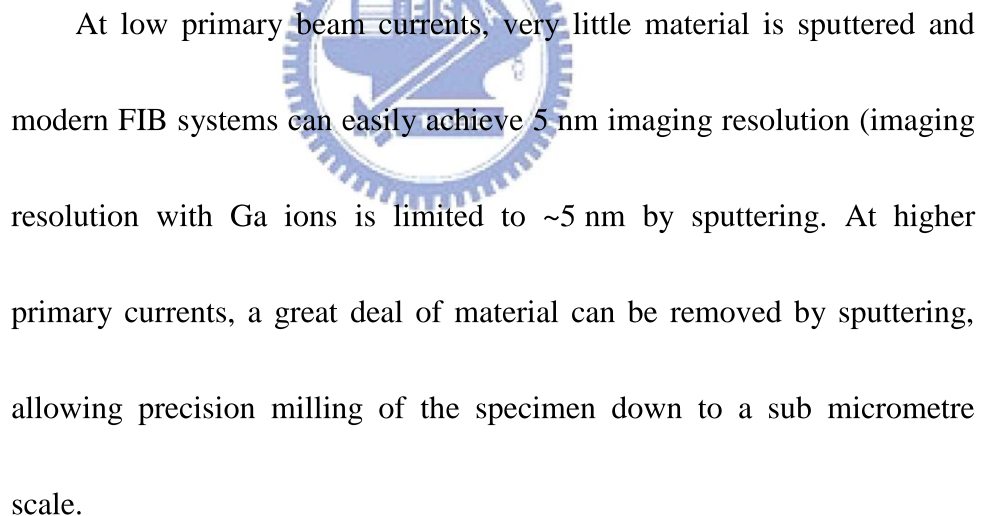

At low primary beam currents, very little material is sputtered and modern FIB systems can easily achieve 5 nm imaging resolution (imaging resolution with Ga ions is limited to ~5 nm by sputtering. At higher primary currents, a great deal of material can be removed by sputtering, allowing precision milling of the specimen down to a sub micrometre scale.

If the sample is non-conductive, a low energy electron flood gun can be used to provide charge neutralization. In this manner, by imaging with positive secondary ions using the positive primary ion beam, even highly insulating samples may be imaged and milled without a conducting surface

coating, as would be required in a SEM.

Until recently, the overwhelming usage of FIB has been in the semiconductor industry. Such applications as defect analysis, circuit modification, mask repair and transmission electron microscope sample preparation of site specific locations on integrated circuits have become commonplace procedures. The latest FIB systems have high resolution imaging capability; this capability coupled with in situ sectioning has eliminated the need, in many cases, to examine FIB sectioned specimens in the SEM.

2.2.3 Inductively coupled plasma reactive ion etching (ICP-RIE)

Reactive ion etching (RIE) is an etching technology used in microfabrication. It uses chemically reactive plasma to remove material deposited on wafers. The plasma is generated under low pressure (vacuum) by an electromagnetic field. High-energy ions from the plasma attack the wafer surface and react with it.

A typical RIE system consists of a cylindrical vacuum chamber, with a wafer platter situated in the bottom portion of the chamber. The wafer

platter is electrically isolated from the rest of the chamber, which is usually grounded. Gas enters through small inlets in the top of the chamber, and exits to the vacuum pump system through the bottom. The types and amount of gas used vary depending upon the etch process; for instance, sulfur hexafluoride is commonly used for etching silicon. Gas pressure is typically maintained in a range between a few millitorr and a few hundred millitorr by adjusting gas flow rates and/or adjusting an exhaust orifice.

Other types of RIE systems exist, including inductively coupled plasma (ICP) RIE. In this type of system, the plasma is generated with an RF powered magnetic field. Very high plasma densities can be achieved, though etch profiles tend to be more isotropic.

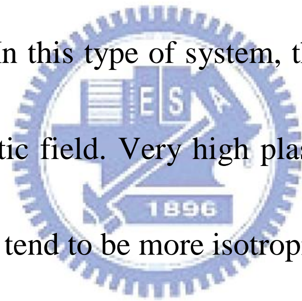

A combination of parallel plate and inductively coupled plasma RIE is possible. In this system, the ICP is employed as a high density source of ions which increases the etch rate, whereas a separate RF bias is applied to the substrate (silicon wafer) to create directional electric fields near the substrate to achieve more anisotropic etch profiles.

Plasma is initiated in the system by applying a strong RF electromagnetic field to the wafer platter. The oscillating electric field

ionizes the gas molecules by stripping them of electrons, creating a plasma. In each cycle of the field, the electrons are electrically accelerated up and down in the chamber, sometimes striking both the upper wall of the chamber and the wafer platter. At the same time, the much more massive ions move relatively little in response to the RF electric field. When electrons are absorbed into the chamber walls they are simply fed out to ground and do not alter the electronic state of the system. However, electrons absorbed into the wafer platter cause the platter to build up charge due to its DC isolation. This charge build up develops a large negative voltage on the platter, typically around a few hundred volts. The plasma itself develops a slightly positive charge due to the higher concentration of positive ions compared to free electrons.

Because of the large voltage difference, positive ions tend to drift toward the wafer platter, where they collide with the samples to be etched. The ions react chemically with the materials on the surface of the samples, but can also knock off (sputter) some material by transferring some of their kinetic energy. Due to the mostly vertical delivery of reactive ions, reactive ion etching can produce very anisotropic etch profiles, which contrast with the typically isotropic profiles of wet chemical etching.

Etch conditions in an RIE system depend strongly on the many process parameters, such as pressure, gas flows, and RF power. A modified version of RIE is deep reactive-ion etching, used to excavate deep features.

2.3 Motivation

Gallium nitride (GaN) and other group III-nitride-based semiconductors have been successfully employed to realize blue light-emitting diodes and blue laser diodes.[30–32] Additionally, due to quantum confinement effects, fabrication and studies of nanostructures have attracted considerable interest for potential application to electronic and optoelectronic devices. With the recent progress in semiconductor process technology, various nanostructure fabrication methods have been investigated such as optical lithography, atomic force microscopy (AFM) machining tools, and metal-catalyzed nanostructure synthesis by a vapour-liquid-solid growth process on different materials.[33-34]

For GaN-based materials, the fabrication and synthesis of GaN nanowires and nanorods using various methods have been reported, for example, carbon nanotube-confined reaction, metal-catalyzed growth

assisted by laser ablation, the high-temperature pyrolysis approach and so on.[35–40] Furthermore, the use of the postgrowth thermal annealing process to induce quantum dots in multiple quantum well layers[41–43] and the photoenhanced wet etching technique to produce GaN whiskers[44–46] was also reported recently. However, all these reported methods are relatively complicated and mostly use the synthesis approach with the aid of catalysts, and there had no mention of the control of the dimension and density of these fabricated GaN nanorods or nanowires.

We study a method to fabricating controllable GaN-based structure dimension and density using no mask by ICP-RIE [47], but the method caused GaN-based structure top-surface was etching and formation high resistance, so unable to fabricating GaN-based light emitting devices. The study of the self-assemble nanometer-sized metal or semiconductor islands has became particularly important recently as it is an attractive method for producing intrinsic nanoscale devices without the need for expensive lithography.

This novel technique to fabricate GaN-based nanorod structure with controllable dimension and density using varying Ni-mask initial layer thickness and inductively coupled plasma reactive ion etching (ICP-RIE).

The size of Ni nano-mask was controled by the thickness Ni film. and rapid thermal annealing condition. The technique offers a relatively simple method for fabrication of controllable mean dimension and density of GaN-based nanorod structure. The experimental details are shown below.

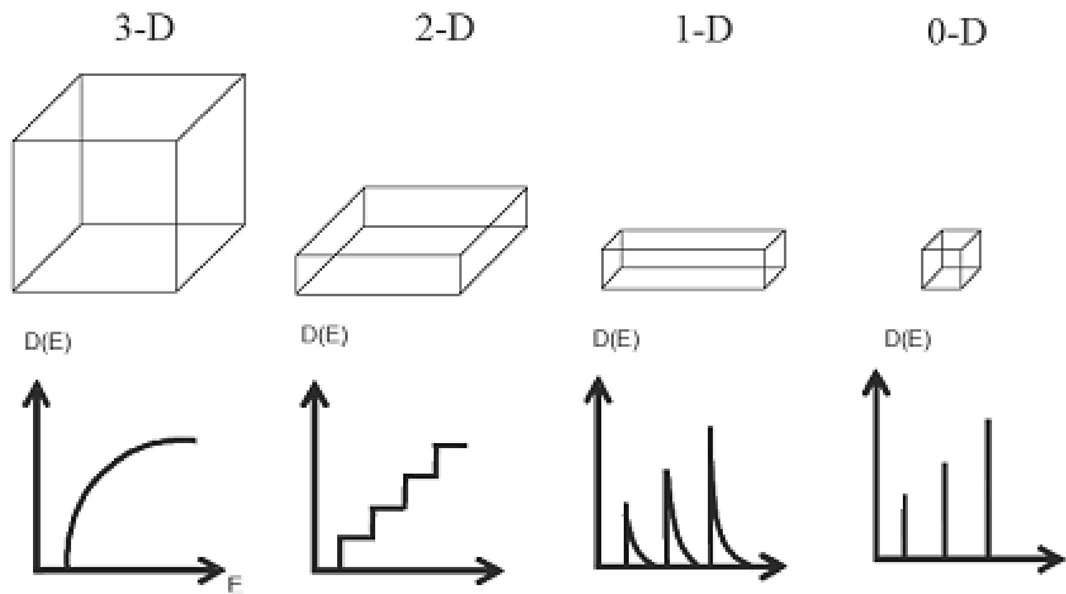

Fig 2.1.1 Dimension of nanostructure and corresponding density of state

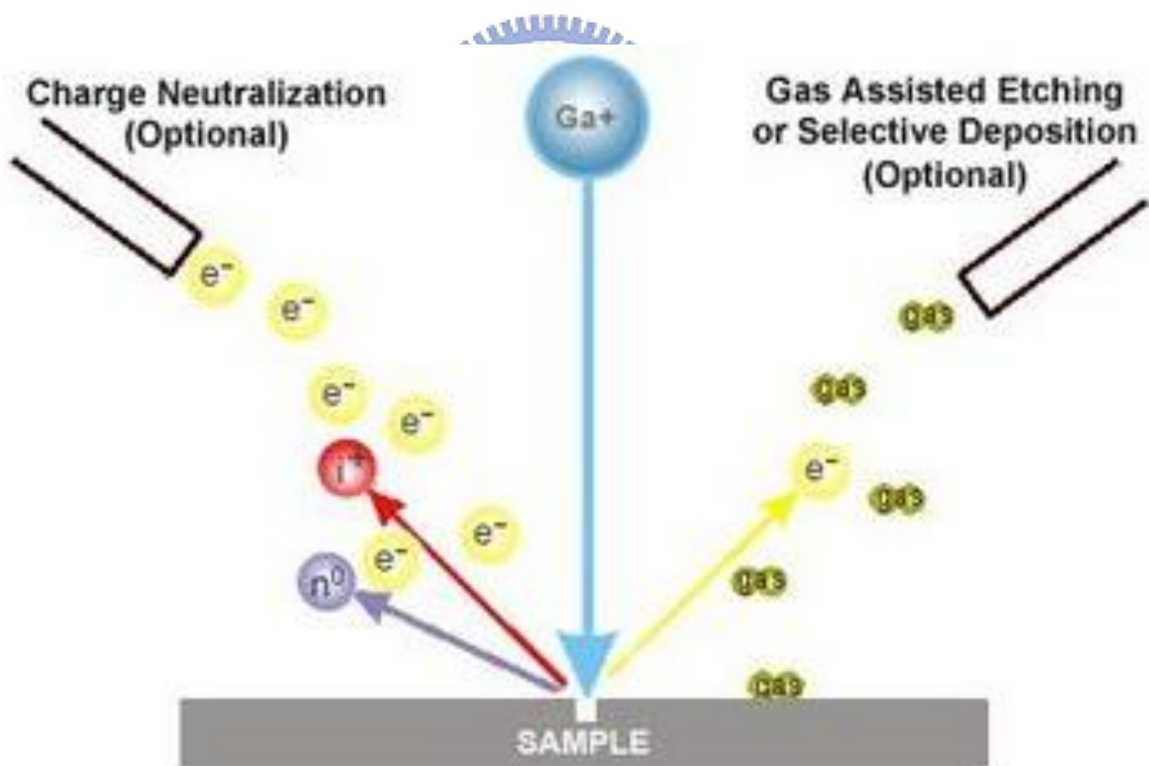

Fig 2.2.2.1 The principle of FIB

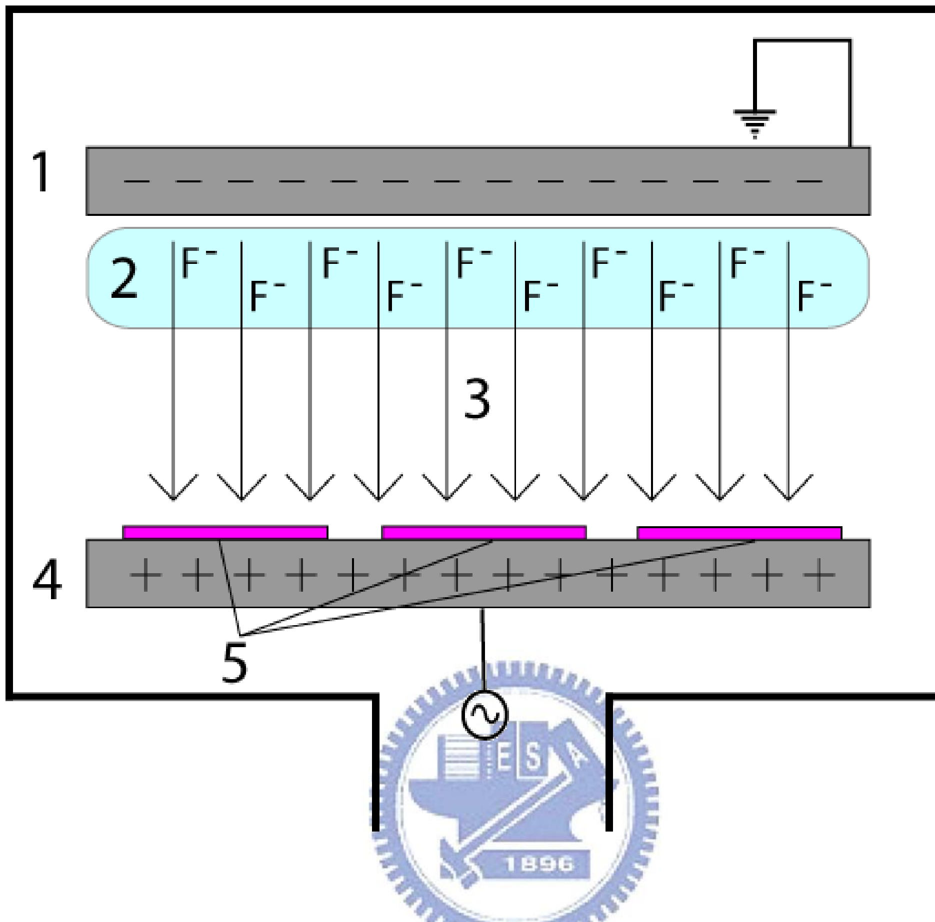

Fig 2.2.3.1 A common RIE setup consists of two electrodes (1 and 4) that create an electric field (3) meant to accelerate ions (2) toward the surface of the samples (5).

2.4 Reference

[1] U. Woggon, Optical Properties of Semiconductor Quantum Dots (Springer, Berlin,1997)

[2] J. K. Sheu, Y. K. Su, G. C. Chi, P. L. Koh, M. J. Jou, C. M. Chang, C. C. Liu, and W. C. Hung, Appl. Phys. Lett., 74, 2340 (1999)

[3] M. A. Reed and W. P. Kirk, Nanostructure Physics and Fabrication _Academic,Boston, (1992)

[4] M. B. Stern, H. G. Craighead, P. F. Liao, and P. M. Mankiewich, Appl. Phys. Lett. 45, 410 (1984).

[5] S. Y. Chou, P. R. Krauss, and P. J. Renstrom, Science 272, 85(1996).

[6] J. Liang, H. Chik, A. Yin, and J. Xu, J. Appl. Phys. 91, 2544 (2002).

[7] M. Park, C. Harrison, P. Chaikin, R. A. Register, and D. H. Adamson, Science 276, 1401 (1997)

[8] Duan and C. M. Lieber, J. Am. Chem. Soc. 122, 188 (2000).

[9] C. C. Chen and C. C. Yeh, Adv. Mater. _Weinheim, Ger._ 12, 738 (2000).

[10] C. H. Liang, L. C. Chen, J. S. Hwang, K. H. Chen, Y. T. Hung,

and Y. F. Chen, Appl. Phys. Lett. 81, 22 (2002).

[11] M. He, I. Minus, P. Zhou, S. N. Mohammed, R. Jacobs, W. L. Sarney, L. Salamanca-Riba, and R. D. Vispute, Appl. Phys. Lett. 77, 3731 (2000).

[12] M. Yoshizawa, A. Kikuchi, M. Mori, N. Fujita, and K. Kishino, Jpn. J.Appl. Phys., Part 2 36, L459 (1997).

[13] E. Calleja, M. A. Sánchez-García, F. J. Sánchez, F. Calle, F. B. Naranjo, E.Munoz, U. Jahn, and K. Ploog, Phys. Rev. B 62, 16826 (2000).

[14] H. M. Kim, D. S. Kim, D. Y. Kim, T. W. Wkang, Y. H. Cho, and K. S.Chung, Appl. Phys. Lett. 81, 2193 (2002).

[15] K. Kawasaki, I. Nakamatsu, H. Hirayama, K. Tsutsui, and Y. Aoyagi, J. Cryst. Growth 243, 129 (2002).

[16] P. Deb, H. Kim, V. Rawat, M. Oliver, S. Kim, M. Marshall, E. Stach, and T. Sands, Nano Lett. 5, 1847 (2005).

[17] Kuball, F. H. Morrisey, M. Benyoucef, I. Harrison, D. Korakakis, and C. T. Foxon, Phys. Status Solidi A 176, 355 (1999).

[18] C. C. Yu, C. F. Chu, J. Y. Tsai, H. W. Huang, T. H. Hsueh, C. F. Lin, and S. C. Wang, Jpn. J. Appl. Phys., Part 2 41, L910 (2002).

[19] I. M. Tiginyanu, V. V. Ursaki, V. V. Zalamai, S. Langa, S. Hubbard, D. Pavlidis, and H. Föll, Appl. Phys. Lett. 83, 1551 (2003).

[20] T. H. Hsueh, H. W. Huang, C. C. Kao, Y. H. Chang, M. C. Ou-Yang, H. C. Kuo, and S. C. Wang, Jpn. J. Appl. Phys., Part 1 44, 2661 (2005).

[21] L. Chen, A. Yin, J. S. Im, A. V. Nurmikko, J. M. Xu, and J. Han, Phys. Status Solidi A 188, 135 (2001).

[22] Y. D. Wang, S. J. Chua, S. Tripathy, M. S. Sander, P. Chen, and C. G. Fonstad, Appl. Phys. Lett. 86, 071017 (2005).

[23] He, L. Chen, Y. K. Song, A. V. Nurmikko, S. R. Jeon, Z. Ren, M.Gherasimova, and J. Han, Phys. Status Solidi C 7, 2740 (2005)

[24] E. D. Harberer et al., Mater. Res. Soc. Symp. Proc. 639, G11.21.1 (2001). 34S. X. Jin, J. Li, J. Z. Li, J. Y. Lin, and H. X. Jiang, Appl. Phys. Lett. 76,631 (2000)

[25] H. W. Choi, C. W. Jeon, M. D. Dawson, P. R. Edwards, and R. W. Martin,IEEE Photonics Technol. Lett. 15, 510 (2003).

[26] A. V. Maslov and C. Z. Ning, Appl. Phys. Lett. 83, 1237 (2003)

[27] J. D. Joannopoulos, R. A. Meade, and J. N. Winn, Photonic Crystals, Molding the flow of Light _Princton University Press,Princeton, NJ, (1995).

[28] E. Yablonowitch, Phys. Rev. Lett. 58, 2059 (1987).

[29] M. Kuball, F. H. Morrissey, M. Benyoucef, I. Harrison, D. Korakakis, and C. T. Foxon , phys. stat. sol. (a) 176, 355 (1999)

[30] S. Nakamura, M. Senoh, N. Iwasa and S. Nagahama: Jpn. J. Appl. Phys.34 (1995) L797.

[31] S. Nakamura, T. Mokia and M. Senoh: Appl. Phys. Lett. 64 (1994) 1689.

[32] S. Nakamura, M. Senoh, S. Nagahama, N. Iwasa, T. Yamada, T.Matsushita, Y. Sugimoto and H. Kiyodo: Appl. Phys. Lett. 70 (1996) 868.

[33] M. T. Bj˝ork, B. J. Ohisson, T. Sass, A. I. Persson, C. Thelander, M.H. Magnusson, K. Deppert, L. R. Wallenberg and L. Samuelson: Appl. Phys. Lett. 80 (2002) 1058.

[34] M. S. Gudiksen, L. J. Lauhon, J. Wang, D. C. Smith and C. M. Lieber: Nature 415 (2002) 617.

[35] W. Han, S. Fan, Q. Li and Y. Hu: Science 277 (1997) 1287.

[36] G. S. Cheng, L. D. Zhang, Y. Zhu, G. T. Fei, L. Li, C. M. Mo and Y. Q.Mao: Appl. Phys. Lett. 75 (1999) 2455.

[37] C. C. Tang, S. S. Fan, M. L. de la Chapelle and P. Li: Chem. Phys. Lett.333 (2001) 12.

[38] X. Duan and C. Lieber: J. Am. Chem. Soc. 122 (2000) 188.

[39] H. Peng, X. Zhou, N. Wang, Y. Zheng, L. Liao, W. Shi, C. Lee and S.Lee: Chem. Phys. Lett. 327 (2000) 263.

[40] W. Q Han and A. Zettl: Appl. Phys. Lett. 80 (2002) 303.

[41] C. C. Chuo, C. M. Lee, T. E. Nee and J. I. Chyi: Appl. Phys. Lett. 76 (2000) 3902.

[42] W. H. Lee, K. S. Kim, G. M. Yang, C. H. Hong, K. Y. Lim, E. K. Suh, H. J. Lee, H. K. Cho and J. Y. Lee: J. Korean Phys. Soc. 39 (2001) 136.

[43] Y. S. Lin, K. J. Ma, Y. Y. Chung, C. W. Liu, S. W. Feng, Y. C. Cheng, C. C. Yang, H. W. Chuang, C. T. Kuo, J. S. Tsang, T. E. Weirich and C.Hsu: Appl. Phys. Lett. 80 (2002) 2571.

[44] C. Youtesy, L. T. Romano and I. Adesida: Appl. Phys. Lett. 73 (1998) 797.

[45] C. Youtesy, L. T. Romano, R. J. Molnar and I. Adesida: Appl.

Phys. Lett.74 (1999) 3537.

[46] P. Visconti, K. M. Jones, M. A. Reshchikov, R. Cingolani, R. J. Molnar and H. Morkoc: Appl. Phys. Lett. 77 (2000) 3532.

[47] C.C. Yu, C.F. Chu, J.Y. Tsai, H.W. Huang, T.H. Hsueh, C.F. Lin,S.C. Wang, Jpn. J. Appl. Phys. 41 (2002) L910.

Chapter 3. Experimental principles and systems

3.1 Gaussian beams

For a Gaussian beam propagating in free space, the spot size w(z) will be at a minimum value w_0 at one place along the beam axis, known as the beam waist as shown in Fig 3.1.1. For a beam of wavelength λ at a distance z along the beam from the beam waist, the variation of the spot size is given by $w(z) = w_0 \sqrt{1 + \left(\frac{z}{z_R}\right)^2}$. where the origin of the z-axis is defined, without loss of generality, to coincide with the beam waist, and where $z_R = \frac{\pi w_0^2}{\lambda}$ is called the Rayleigh range.

At a distance from the waist equal to the Rayleigh range z_R, the width w of the beam is $w(\pm z_R) = w_0\sqrt{2}$ The parameter w(z) approaches a straight line for $z \gg z_R$. The angle between this straight line and the central axis of the beam is called the divergence half-angle of the beam. It is given by $\theta \simeq \frac{\lambda}{\pi w_0}$ (θ in radians.). The total angular spread of the beam far from the waist is then given by $\Theta = 2\theta$.

The Gaussian Beam is an idealization that is only approximately met, even in well-designed laser systems. A measure of the quality of an optical beam is the deviation of its profile from Gaussian form. For a beam of waist diameter $2W_m$ and angular divergence $2\theta_m$,a useful numerical

measure of the beam quality is provided by the M^2-factor,which is defined as the ratio of the waist-diameter-divergence product,$2W_m \cdot 2\theta_m$ (usually measured in units of mm•rad),to that expected for a Gaussian beam ,which is $2W_0 \cdot 2\theta_0 = 4\lambda/\pi$.Thus,

$$M^2 = \frac{2W_m \cdot 2\theta_m}{\frac{4\lambda}{\pi}}$$

If the two beams have the same waist,the M^2-factor is simply the ratio of their angular divergences,

$$M^2 = \frac{\theta_m}{\theta_0}$$

Where$\theta_0 = \lambda/\pi W_0 = \lambda/\pi W_m$.Since the Gaussian beam enjoys the smallest possible divergence angle of all beams with the same waist diameter,$M^2 \geqq 1$.The specification of the M^2-factor of an optical beam thus signifies a divergence angle that is M^2 times greater than that of a Gaussian beam of the same waist diameter. [1]

3.2 Knife Edge

The knife-edge method is a commonly used technique to characterize the optical profiles of laser beams or focused spots. As the knife-edge intersects the beam in a direction perpendicular to the propagation axis of the beam, a photodetector measures the intensity of the

unmasked portion of the beam. If the spatial profile of the laser beam is described by a Gaussian line shape, the signal measured by the detector is represented by an integrated Gaussian function. In principle, the beam diameter can be determined from such photodetector data.

In a scanning knife edge system as shown in Fig. 3.2.1, a sharp knife edge plate scans across an optical field distribution[2][3] . The photo detector placed behind the plate detects the partial optical energy which is not blocked by the plate. The optical intensity I(x) measured by the photo detector,and it can be described with a Gaussian function of the knife edge position x is given by:

$$\begin{aligned} I(x_b) &= \frac{2P}{\pi w^2} \int_{-\infty}^{x_b} e^{-2\frac{x^2}{w^2}} dx \int_{-\infty}^{\infty} e^{-2\frac{y^2}{w^2}} dy \\ &= \frac{P}{w}\sqrt{\frac{2}{\pi}} \int_{-\infty}^{x_b} e^{-2\frac{x^2}{w^2}} dx \\ &= \frac{P}{w}\sqrt{\frac{2}{\pi}} \int_{-\infty}^{x_b} P(x) dx \end{aligned} \qquad (3.2.1)$$

where P(x) is the optical field distribution,and w is the distance from the beam axis where the intensity drops to $1/e^2$(~13.5%) of the maximum value. This response can be normalized to the total integrated signal of the full totally unmasked beam ($x_b \to \infty$) by

$$\tilde{I}(x_b) = (\frac{1}{w}\sqrt{\frac{2}{\pi}}) \int_{-\infty}^{x_b} e^{-\frac{2(x-x_0)^2}{w^2}} dx \qquad (3.2.2)$$

where Eq.(3.2.2) represents the normalized response function

In principle, w,which determines the ultimate value for the beam radius, can be deduced from the transformation condition which converts Eq. (3.2.3) into the normal distribution:

$$N(z) = \frac{1}{\sqrt{2\pi}} \int_{-\infty}^{z} e^{-\frac{u^2}{2}} du \qquad (3.2.3)$$

The salient difference between $\tilde{I}(x_b)$ and N(z) is found in the arguments of the exponents in the integrands. The two arguments can be made equal if the condition

$$\frac{2(x-x_0)^2}{w^2} = \frac{u^2}{2} \;,\; x = \frac{w}{2}u + x_0$$

From a normal distribution table,the values of u at which the normal distribution N(z) equals 0.1 and 0.9 are found to be ±1.28. This information provides two simultaneous equations:

$$x_{10} = \frac{w}{2}(-1.28) + x_0$$

$$x_{90} = \frac{w}{2}(1.28) + x_0$$

which when solved yields, $w=0.78125(x_{90}-x_{10})$

If the field distribution is a Gaussian spot, we can get the data by varying knife's position x, as shown in Fig. 3.2.2.The beam radius of laser can also be inferred from the distance between 10% and 90% of the full scale measured normalized I(x),and multipled a factor 0.78125,i.e.

$w=0.78125(x_{90}-x_{10})$.Focused optical spot profile measurement is demonstrated.

3.3 Microphotoluminescence spectroscopy (μ-PL)

Photoluminescence (PL) spectroscopy has been used as a measurement method to detect the optical properties of the materials because of its nondestructive characteristics. PL is the emission of light from a material under optical excitation. Reducing the laser beam spotsize to micrometer by beam expanders and objective lens is the so-called μ-PL. The laser light source used to excite carriers should have larger energy band gap than the semiconductors. When the laser light is absorbed within the semiconductors, it would excite the carriers from the valence band to the conduction band. Then, it produces the electrons in the conduction band and the holes in the valence band. When the electron in an excited state return to the initial state, it will emit a photon whose energy is equal to the energy difference between the excited state and the initial state, therefore, we can observed the emission peak from PL spectrum.

The schematic setup of our μ-PL system is shown in Fig. 3.3.1. The pumping source is Nd:YAG 355 pulsed laser with a pulse width of ~1nsec

at a repetition rate of 1KHz.The PL is collected by a 15X objective lens and straightly collected by spectrometer with a charge-coupled device (Jobin-Yvon IHR320 Spectrometer) or collected by a fiber with 200μm core,which rotating in the normal plane of the sample,and also coupled into spectrometer. The spectral resolution is about 0.07nm for spectral output measurement.We can also monitor the image and spatial distribution on the sample surface by charge-coupled device (CCD) and beam view,respectively.

3.4 Pumping power density and spotsize calculation

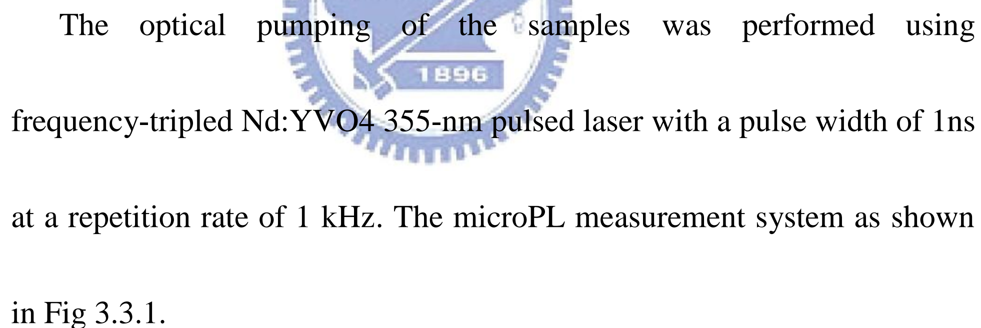

The optical pumping of the samples was performed using frequency-tripled Nd:YVO4 355-nm pulsed laser with a pulse width of 1ns at a repetition rate of 1 kHz. The microPL measurement system as shown in Fig 3.3.1.

It is often necessary to calculate the power density (Power/Area) of a laser beam (for example, when trying to determine whether a beam will damage an optic or detector).Power density is expressed in watts per square meter (W/m^2) or milliwatts per square centimeter (mW/cm^2). Usually power density is more often expressed in terms of W/cm^2 when making surveys. In our experiments, the pumping power density can be

presented by following equation

$$\mathbf{Power\,Density} = \frac{P_{average} \times \frac{1\,msec}{1\,nsec} \times 0.3 \times \alpha}{\pi (M^2 R)^2} \qquad (3.4.1)$$

where $P_{average}$ is the laser optic power measured by power detector, 0.3 is the value of calibration when passing through the 15X objective lens. And,α (=0.85) is the absorption coefficient of the GaN, R is the radius of the laser beam in centimeters.M^2(=1.3) is defined as the ratio of the waist-diameter-divergence product,$2W_m \cdot 2\theta_m$ (usually measured in units of mm・rad),to that expected for a Gaussian beam.

Specification of laser shows the full angle is 3mrad,beam waist location is -135mm and M^2 is 1.3,so that initially spotsize which is 75.37μm can be obtained by using equation 3.4.2

$$\omega_0 = \frac{\lambda}{\pi \theta} \qquad (3.4.2)$$

The distance between laser and objective lens is about 121.7cm, according to equation 3.4.3 and 3.4.4, spotsize expands to 1.83mm , then be focused to 0.8μm by a 15X objective lens which focal length was 13mm by using equation 3.4.5.

$$Z_0 = \frac{\pi \omega_0^2}{\lambda} \qquad (3.4.3)$$

$$\omega_1 = \omega_0 \times \sqrt{1+\left(\frac{Z}{Z_0}\right)^2} \qquad (3.4.4)$$

$$\omega_2 = \frac{\lambda f}{\pi \omega_1} \qquad (3.4.5)$$

In other words,the theoretical model of laser beam spotsize calculation results indicated that the value of beam radius is 0.8μm, Rayleigh range is 5.73μm and the diverge half-angle is 0.14 rad after going through 15X objective lens.

In order to know the real beam raidus, we use Knife Edge experiment to measure Nd:YVO4 355nm pulsed laser. Under a fixed excited power ,we can get the relationship of normalized intensity v.s. distance that the knife moved, as shown in Fig.3.4.1(a). The distance between 10% and 90% of full scale needs to multiple a factor of 0.78125, and the value is the called spot size. We have presented some knife edge results obtained on measurements of various Z axis value. For example, when moving knife away from the objective lens focal point about Z=25μm, the spotsize will be attained 4.6um as shown in Fig.3.4.1(b).

Vary objective lens distance Z from -125μm to 325μm, then we can obtained Gaussian beam curves of the laser, and its diverge half-angle is 0.147 rad. The calculation of Nd:YVO4 pulsed laser beam spotsize is very similar to our experimental results . The comparison between calculation

results and experimental results as shown in Fig.3.4.2. and Table 3.4.1

3.5 Scanning electron microscope (SEM)

The electron microscope uses electromagnetic lenses to focus the beam to produce an image. However, SEM and TEM differ in the way images are produced and magnified. SEM is used to view the surface or near surface of a sample, whereas TEM provides information of the internal structure of thin specimens. The scanning electron microscope as the name suggests scans across the specimen by the scan coils.

As the sample is scanned by the electron beam, it emits electrons and electromagnetic radiation. A detector counts the low energy secondary electrons (< 50 eV) or other radiation emitted. The image is produced by two dimensional intensity distributions by scanning a cathode ray tube (CRT) spot onto a screen and modulating the brightness by the amplified current from the detector. Three dimensional samples change the way electrons are emitted and results in the appearance of a three dimensional image. Resolutions less than 1 nm may be achieved.

3.6 Transmission electron microscope (TEM)

TEM is a method of imaging where a beam of electrons are directed through a sample after which they are scattered into discrete diffracted beams. The diffracted electron beams are then focused in the back focal plane of the objective lens. TEM may have two modes. When operated in diffraction mode, the diffraction lens is focused on the back focal plane to produce a diffraction pattern. For the imaging mode, the diffraction lens is focused on the first image plane to produce a magnified image. In addition, the beam may be allowed to pass through the sample to obtain a bright-field image however the diffracted beams produce a dark-field image.

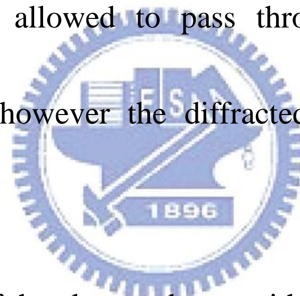

The interaction of the electron beam with crystalline material tends to be by diffraction. The orientation of the planes of atoms in the crystal to the electron beam changes the intensity of diffraction. TEM equipment often uses a goniometer to allow the sample to be tilted to a range of angles to obtain specific diffraction conditions. Diffracted electrons are also selected using different apertures.

The intensity of diffraction is a maximum at the Bragg angle, although a variation of diffraction intensity occurs with deviation from the Bragg

angle. This also depends on the thickness of the specimen. The thinner the crystal sample, the further the crystal may deviate from the Bragg condition.

When crystal planes are almost parallel to the electron beam they are close to fulfilling Bragg's Law. The majority of electrons are diffracted when the electron beam strikes one set of lattice planes exactly at their Bragg angle and only a few will pass through the sample undeviated. If the planes are exactly at the Bragg condition, strong diffraction will occur and the bright field image will appear dark.

This variation with diffraction is shown with bend contours which are a feature of bending of the crystal planes. Dark contour images correspond to regions at the Bragg angle, while light contours result in the regions not strongly diffracting.

3.7 Charge Coupled Device (CCD) camera

A charge-coupled device (CCD) is a device made up of semicondutors that enables the transmission of analog signals (electric charges) through successive stages (capacitors), controlled by a clock signal. "CCD" refers to the way the image signal is read out from the chip.

Under the control of an external circuit, each capacitor can transfer its electric charge to one or other of its neighbors. CCDs can be used as a form of memory or for delaying samples of analog signals.Today, charge-coupled devices are most widely used in arrays of photoelectric light sensors, to serialize parallel analog signals. CCDs are used in digital photography, astronomy, sensors, electron microscopy , medical fluoroscopy, and optical and UV spectroscopy

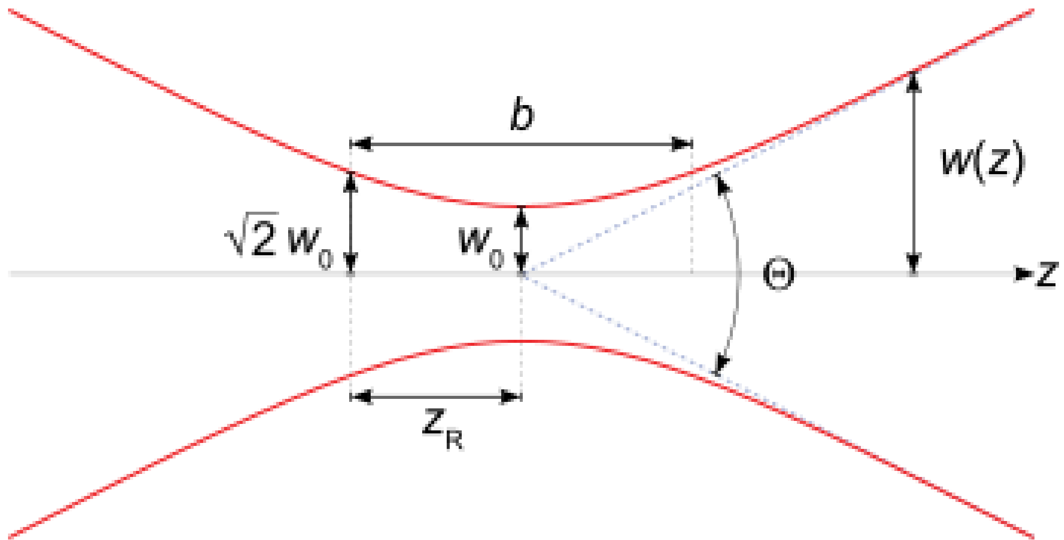

Fig.3.1.1 Gaussian beam

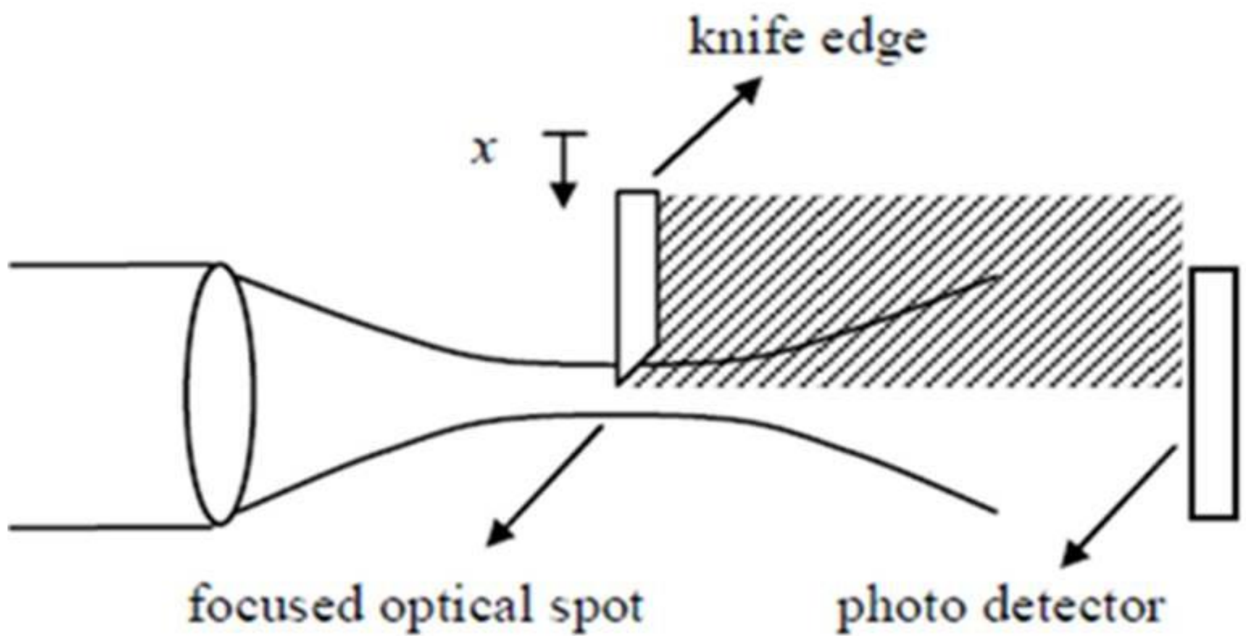

Fig. 3.2.1 Schematic of a scanning knife edge

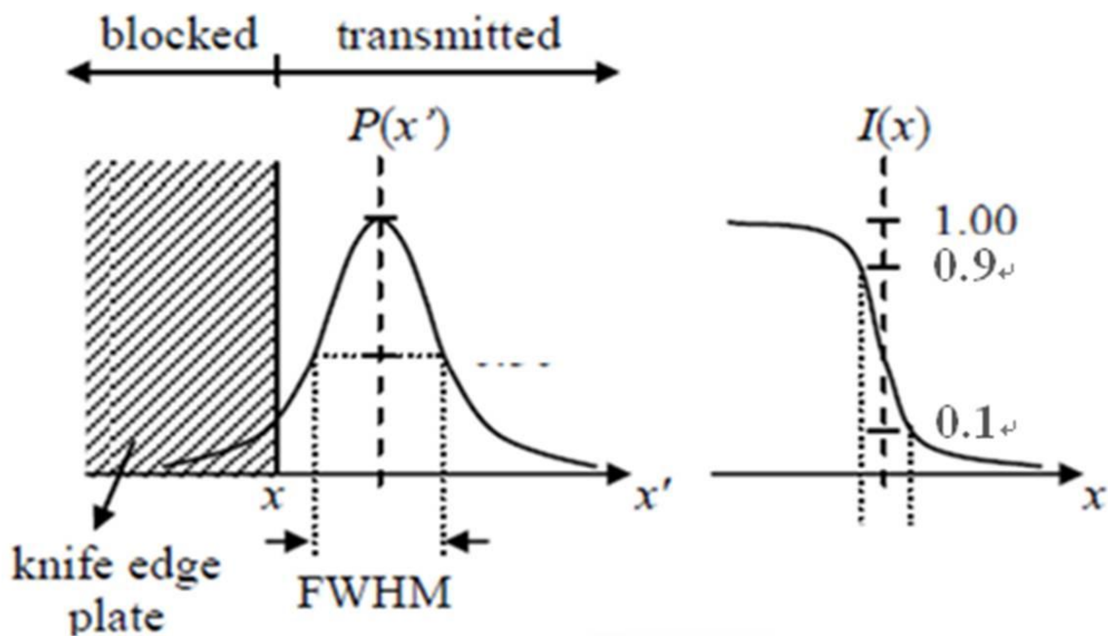

Fig. 3.2.2 Spot profile and measured signal

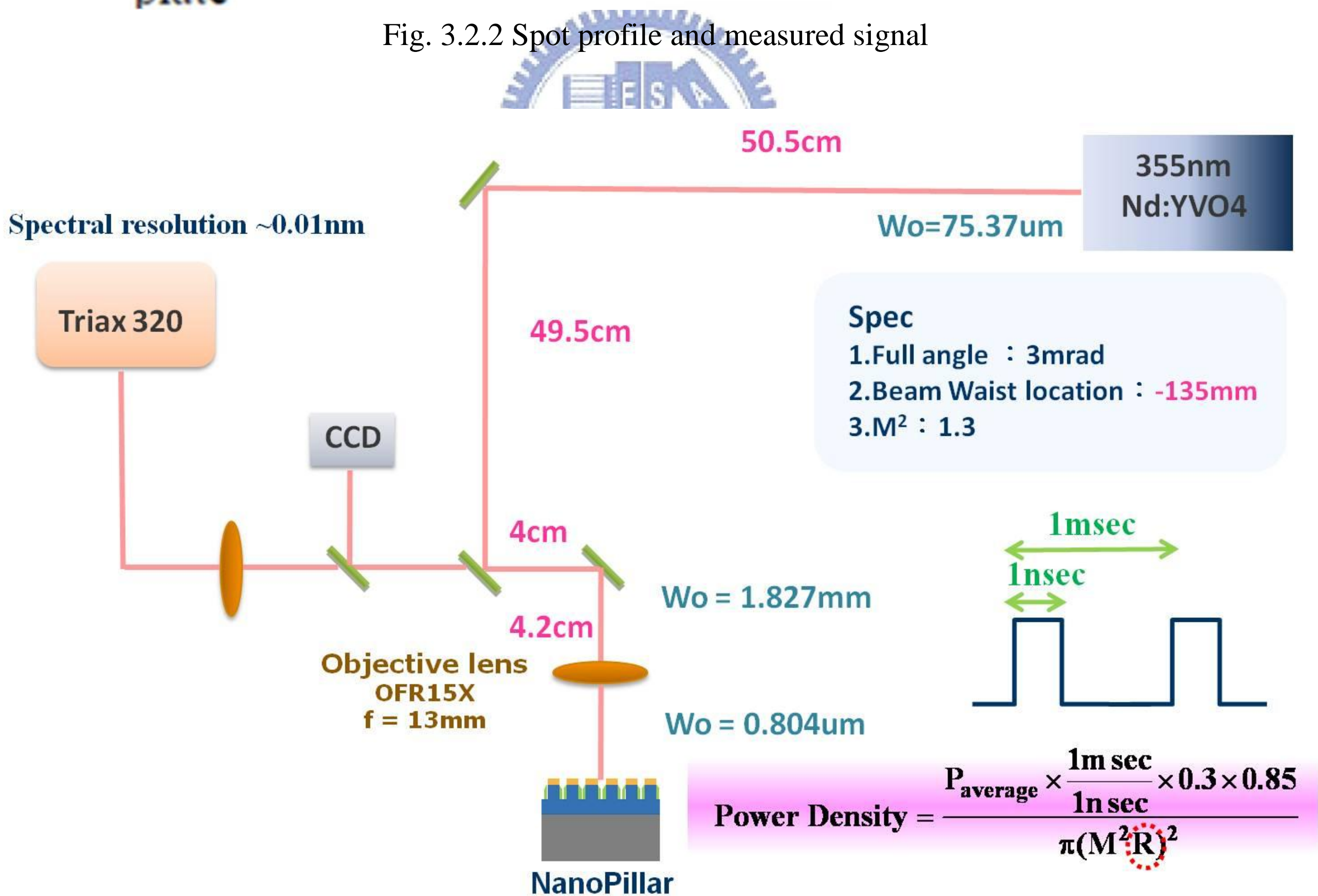

Fig 3.3.1 Nd:YVO4 355-nm pulsed laser microPL measurement system

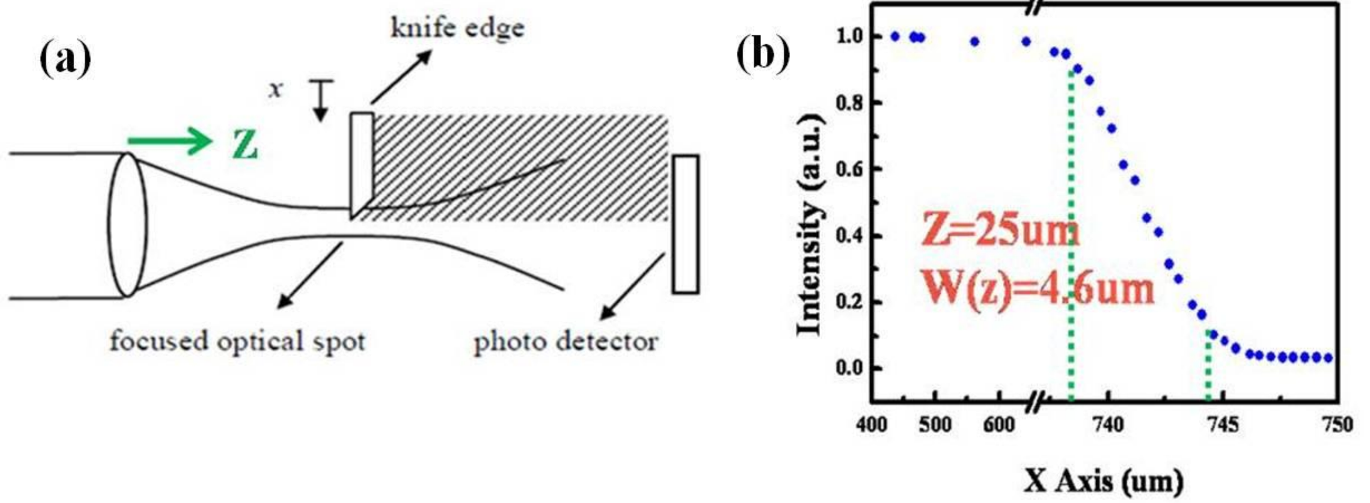

Fig.3.4.1. (a) Knife Edge measurement diagram (b) the distance between lens and knife is 25μm,and laser beam spotsize is about 4.6μm

	W_0 (μm)	Θ(rad)	Z_R (μm)
Theory	0.8	0.141	5.73
Experiment	1.75	0.147	27.35

Table 3.4.1 Comparison of calculation results and experimental results

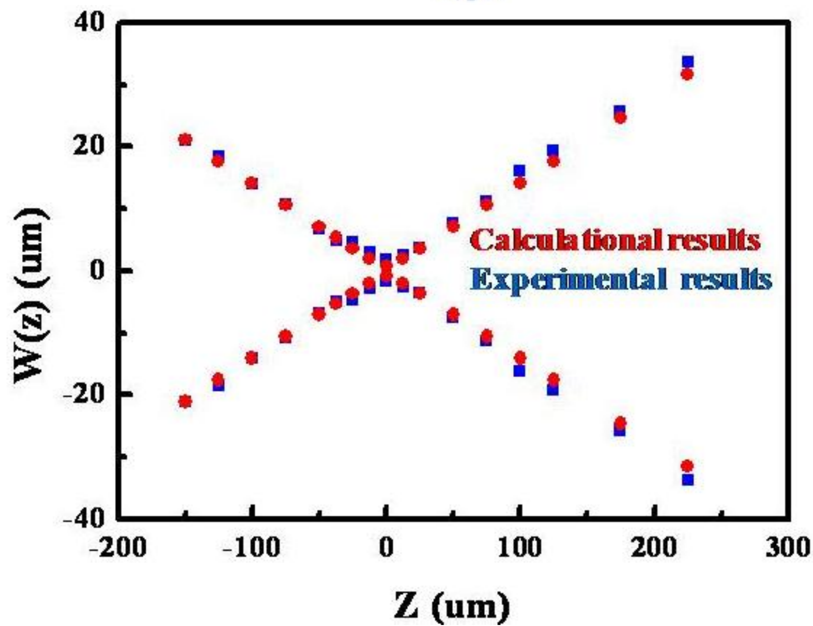

Fig.3.4.2. Laser spotsize calculation and experimental results by knife edge measurement

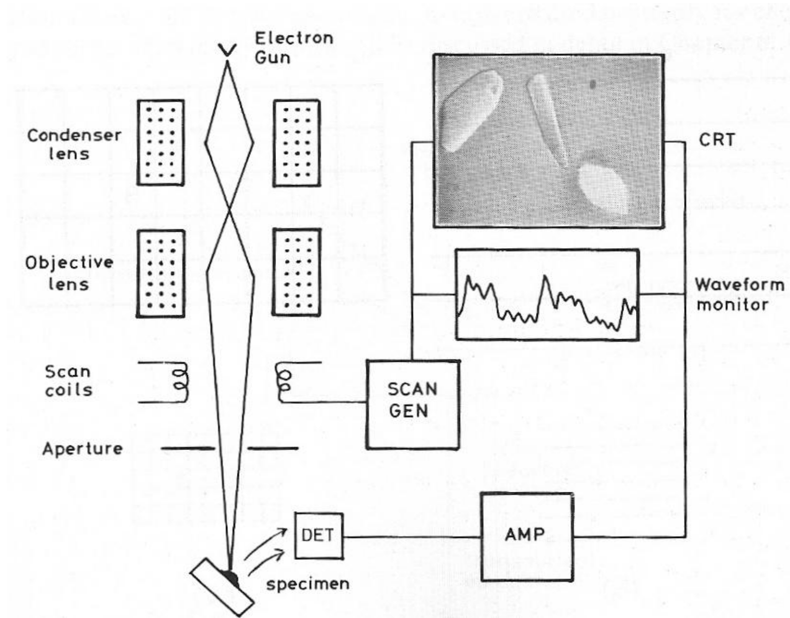

Fig. 3.5.1 Schematic diagram of a scanning electron microscope

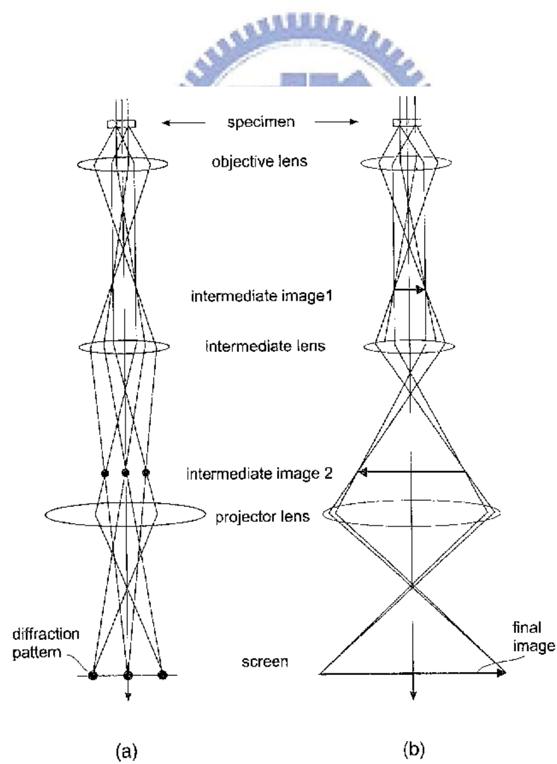

Fig. 3.6.1 Ray diagram showing two basic operations of TEM [2]

The ray diagram (Fig. 3.5.1) shows (a) imaging projecting a diffraction pattern and (b) projection of an image onto a viewing screen.

3.8 Reference

[1] ”Fundamentals of Photonics 2ed” B.E.A Saleh,M.C. Teich (2007)

[2] Yi Chiu, Jiun-Hung Pan, 15, No. 10, OPTICS EXPRESS 6373 May. (2007)

[3] John M. Khosrofian and Bruce A. Garetz,APPLIED OPTICS, 22, No. 21, Nov. (1983)

Chapter 4. Fabrication and Characteristics of Optically Pumped Nitride-Based nanopillars

GaN 1-D nanostructure (i.e. nanorods、nanowires and nanopillars) have potential to increase light extraction efficiency of light emitting devices and reduce the quantum confine stark effect in strain relaxed GaN multiple quantum wells devices. In addition, the 1-D GaN nanowires structure have been shown that it can function as optical waveguides and Fabry-Perot cavities for strong light confinement and coherent feedback [1, 2]. Its cavities typically have a small size with diameters ranging from 10 to 100 nm and lengths ranging from 0.5 to 40 μm and a large refractive index contrast between GaN (n=2.5) and air (n=1). The room temperature optically pumped GaN nanowire lasers have been demonstrated [2, 3]. For the synthesis of GaN 1-D nanostructure, bottom-up and top-down approaches have been developed on GaN nanowire or nanorod structure by MOCVD、HVPE and RF-MBE systems. The GaN nano structure devices can be fabricated by top-down approach, which employs nano mask and etching, or bottom-up approach, which relies on nano scale crystalline growth. The top-down approach [4] has better control on patterning but the etching process often induces surface defects. The bottom-up approach [5], on the contrary, has less control on over all patterning but often produces

crystalline GaN facets on the sidewalls with much less defects. In this chapter, we report the fabrication of hexagonal crystalline nanopillars and observation observation of room temperature lasing action form an optically pumped GaN nanopillars The nanopillars were fabricated using self-assembled Ni as nanomask and ICP-RIE etching followed by crystalline regrowth of nanopillar formed wafer

4.1 Fabrication of hexagonal GaN Nanopillars

The schematic of fabrication process flow is shown in Fig. 4.1.1(a)-(d). The sample with a 3μm GaN buffer layer is grown on a c-plane sapphire (0001) substrate by low pressure metal organic chemical vapor deposition(MOCVD). First, a 300 nm Si_3N_4 thin film is deposited on the GaN buffer layer by plasma-enhanced chemical-vapor deposition system, followed by electron-beam evaporation of a 100 nm Ni metal film as illustrated in Fig. 4.1.1(a). The as grown sample is subsequently subjected to rapid temperature annealing at 850 °C under a nitrogen ambiance for 1 min. to form self-assembled Ni nano masks on Si_3N_4 film surface as shown in Fig. 4.1.1 (b). A reactive ion etching is conducted to etch Si_3N_4 film using a CF_4/O_2 gas-mixture to transfer Ni nano mask pattern down to

Si_3N_4 layer. The sample is subsequently etched down to the GaN buffer layer by the ICP-RIE system (SAMCO ICP-RIE 101iPH) operated at 13.56 MHz under a gas mixture of Cl_2/Ar = 50/20 sccm with 2 mins. of etching time to form nanopillars as shown in Fig. 4.1.1(c). The ICP source power, bias power and the chamber pressure of the ICP-RIE system are set at 400/100 W. The sample is dipped into a nitric acid solution (HNO_3) at 100 ◦C for 5 min. to remove the Ni nano masks. Finally, the GaN nanopillar provides seed layer for epitaxial regrowth, which grows a GaN passivation layer on the sidewalls of etched GaN nanopillars as shown in Fig. 4.1.1 (d).

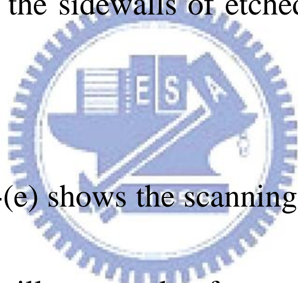

Figure 4.1.2(a)-(e) shows the scanning electron microscope images of as grown GaN nanopillars sample after regrowth process. Self-assembled Ni nano masks on Si_3N_4 film surface as shown in Fig. 4.1.2(a), and it's diameter is about 100nm. Fig. 4.1.2 (b) shows nanopillars etched down by ICP-RIE then were removed the Ni nano maskd. The Fig. 4.1.2 (c) is the top view of nanopillars showing hexagonal crystalline sidewall facets and the hexagonal nanopillar density about ~$8.5x10^5/cm^2$. Various nanopillar with different diameter from 200nm to 300nm were prepared by using self-assembled different size Ni nano masks. At the top of each nanopillar,

there is GaN slightly growing over Si_3N_4 mask showing inclined {1102} facets as shown in Fig. 4.1.2(d). The diameter and height of nano-pillars are about 250 nm and 660 nm, respectively, as shown in Fig. 4.1.2 (e).

4.2 Characteristics of Optically Pumped Nitride-Based nanopillars

4.2.1 Optical pumping of GaN nanopillars at room temperature

The as grown sample is evaluated under optical pumping of excitation density from 2.47MW/cm^2 to 19.8MW/cm^2,using Nd:YVO4 355nm pulsed laser with pulse width ~1ns at a repetition rate of 1 kHz ; the excited laser beam spotsize is ~13.5μm. The light emission from the sample was collected using an imaging optic into a spectrometer/cooling charged device (Jobin-Yvon Triax 320 Spectrometer) with a spectral resolution of 0.01nm.

The Fig. 4.2.1.1 shows the emission spectra at different pumping density. The spontaneous emission of as grown sample below threshold was located at around 365 nm. With pumping intensity increasing, it is interesting to see the emergence of a peak at 369nm. Figure 4.2.1.2 shows the measured emission intensity and linewidth as function of pumping intensity. The laser emission spectral linewidth reduces with the pumping intensity above the threshold energy and approaches ~ 0.9 nm above the

pumping intensity of 15MW/cm^2. The solid line represents a linear fit to the experimental data ; the threshold excitation density is ~12.4 MW/cm^2.

Under laser spot size about 37.1μm ,we repeat the measurement results from etched nanopillars, etched nanopillars without passivation (Ref) and bulk samples included. In Fig.4.2.1.3, it is fascinating to see such a stimulated emission from passivated nanopillars, where as etched pillars without passivation and bulk GaN samples do not show such stimulated emission. The threshold power density of nanopillars is about 2.5MW/cm^2 and etched pillars without passivation is 3.6MW/cm^2. In other words, gain of nanopillars is higher than Ref sample. The gain depends on radiated recombination. We suggest that the nanopillars surface after regrowth have better quality and improve radiated recombination effect. As the pumping power density increases, the full width at half maximum (FWHM) also gets narrower.

Meanwhile the investigation of the characteristics of the nanopillars has gradually attracted more attentions. Kako *et al.*investigated the coupling efficiency of spontaneous emission (β) . In order to understand the β of this sample,we normalized the vertical scale of Fig.4.2.1.4 and repoltted it in a semilogarithm scale,as shown in Fig.4.2.1.5. According to

[6] , the difference between the heights of the emission intensities before and after the threshold correspond roughly to the value of β. The β value of nanopillars and etched nanopillars without passivation (Ref) is about 4.1×10^{-2} and 2.7×10^{-2}. We suggest that the rough surface of Ref sample might cause light scattering. These indicate that the low threshold and high coupling efficiency in hexagonal GaN nanopillars sample due to the reduction of surface defect on the sidewall after regrowth process.

4.2.2 Lasing characteristics under different pump spotsize

Meanwhile, we measured the power dependent PL of nanopillars with various pumping laser beam spotsize between 1.3μm to 13.52μm. The Fig.4.2.2.1 (a)~(d) shows the PL spectra under different pump spot size and pumping intensity. We observed that the lasing behaviors change dramatically from small spotsize to large size (1.3μm to 13.52μm). At optical pumping with small spot size condition (spot size~1.27μm), the emission spectrum has several satellites peaks above the threshold power density. The dominated lasing peak was located at 363 nm and the mode spacing roughly equated to 1nm. With the spot size increase, the multiple peaks in lasing spectra cannot be resolved when the pump spot size large than 6.7μm.

Fig 4.2.2.2 shows different spotsize emission intensity v.s pumping intensity. It is interesting to see non-linear increase of peak besides the linear increase of broad emission. The threshold pumping density with spotsize from 1.27μm to 13.52μm (1.27μm,3.3μm,6.65μm,13.5μm) is 168MW/cm^2, 85.6MW/cm^2, 21.5MW/cm^2, 12.4 MW/cm^2 , respectively. As spotsize increasing, threshold power density get decreasing. We suggest that more pillars pumped under larger spotsize, and the increasing material gain cause decreasing threshold power denity.

As excitaion spotsize increasing, the central position of lasing peak wavelength was gradual red-shift, and mode spacing got decreasing and the number of lasing multi-peak modes dreased, as shown in Fig. 4.2.2.3. We suggest that the increasing number of multi-mode might depend on increasing material gian under larger spotsize. About spot size ~6.7μm, we can find that the number of lasing peak seems one, i.e. single peak, maybe the multi-mode were mixed together. Further detail investigations will be reported.

These experimental data are poltted as Fig.4.2.2.4. It indicated that as spotsize increasing from 1.3μm to 13.5μm, threshold power dreased from 168 MW/cm^2 to 9.9MW/cm^2, and peak wavelength red-shift from

363nm to 369nm. In Fig.4.2.2.5., when the spotsize becomes larger, the nanopillars PL spectra shows increasing mode numbers, and decreasing mode spacing.

Furthermore,we try to figure out this phenomenon is dependent on spotsize or not. Fig 4.2.2.6 (a) shows near threshold gain spectra of GaN nanopillars under optical pumping with different spot size. The gain spectrum of as grown sample with a large pump spot size was dominated by a board peak from the 356 nm to 380 nm, which consists of one peak at 363 nm and another peak around 368 nm. In the board gain spectrum, the PL peak at 363 nm is assigned to the hexagonal GaN bound exciton. Several reports have indicated that the PL peaks of GaN sample from 364 nm to 368 nm have been attributed to the near band edge states. The emission peak at 368 nm will blue shift until it overlaps to the GaN bound exciton peak when the spot size under tight focusing conditions. We observed that the peak shift effect is not related to the pumping power intensity under change of spot size condition. We also suggest that the peak shift effect of lasing peak was attributed to the change of material gain spectrum under different pumping condition.

4.2.3 Angle resolved PL

In order to confirm the modulation in azimuthally isotropic irradiance of GaN bulk and nanopillars, the irradiance measurement is carried out by using an angular-resolved photoluminescence (PL) configuration. The system of angle-resolved μ-PL measurement as illustrated in Fig.4.2.3.1, the setup consists of Nd:YVO4 laser of 355 nm, an object lens of 15X magnification, and a fiber with a collimator.

Our samples can be pumped by using Nd:YVO4 laser of 355 nm, the focusing beam of laser with a diameter about 4.3 μm is normal incident to the surface of sample. The most part of emitting light radiated from the inner of sample would couple into the air through the proposed structure surface. The fiber in an angular-resolved irradiance measurement is adopted to collect the spatial emitting light. The N.A. value of 39X objective lens is about 0.5. This angular-resolved irradiance measurement system is convenient to get the emitting light pattern of LEDs for photoluminescence configuration.

The optical spectra of the GaN bulk sample were recorded with a beam normal incident and the emission collected in the angle of 60° ~ -60° to the sample surface. We observed that the emission peak wavelength of the GaN bulk is similar under same laser excitation , however, the emission

peak intensity will decrease gradually under large angle. We plot emission intensity of bulk sample as a function of collect angle as shown in Fig.4.2.3.2(a), which reveals that the GaN bulk is isotropic scatter (or Lambertion radiation).

In comparison, we also measured the angle-resolved μ-PL diagrams of lasing mode of nanopillars, the lasing emission peak wavelength of nanopillars also similar under varing collect angle as shown in Fig 4.2.3.2(b). It can obviously observed that the nanopillars emission intensity have different emission anlges corresponding to the normal direction (10˚, -15˚) respectively. Perhaps the top surface like house roof on the pillar structures help to redirect the radiation toward sapphire substrate to the front surface direction, and the light output coupled out in some direction.

4.3 Temperature dependent threshold and characteristic temperature

Besides the basic characteristics of nanopillars at room temperature, we also investigated the behavior of the nanopillars under varing temperature. The temperature was lowered by using liquid nitrogen and controlled by the thermo controller.

Temperature dependence of the μ-PL spectra at various injection current levels has been measured between 77 and 322 K,and the laser beam spotsize is about 14μm.

As we can see in Fig.4.3.1 , there exists stimulation emission peak at 359nm at 77K, and threshold pumping power density ~ 8MW/cm^2. However, with further decrease of temperature of temperature down to77K, significant blue-shift from 370nm to 359nm of the emission peak wavelength and decreasing threshold power density is observed. The blue-shift peak wavelength of nanorods maybe due to equation 4.3.1

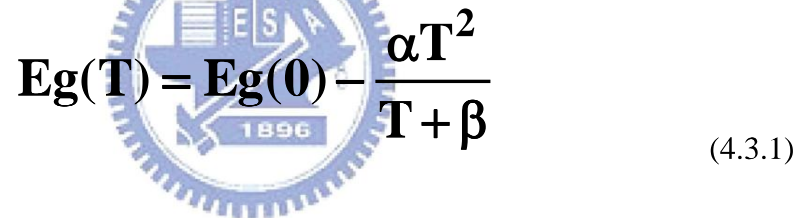

$$\mathbf{Eg(T) = Eg(0) - \frac{\alpha T^2}{T + \beta}} \tag{4.3.1}$$

The emission intensity-excitation power curve at 77K, 252K, and 322K are shown in Fig.4.3.2. It was observed that the increase in temperature leads to an increase in threshold excitation energy. It is due to the increase of non-radiated recombination and decrease of radiated recombination. In other words, the internal quantum efficiency is decreased. The gain depends on the radiated recombination. Therefore, the higher temperature decreases gain and leads to an increase in stimulated

emission threshold.

The temperature dependent threshold excitation energy as shown in Fig.4.3.3 , the solid line inrepresents the best fit of the experimental data to the empirical form $I_{th}(T)=I_0exp(T/T_0)$, where I_{th} is the threshold excitation energy, I_0 is a constant, T is the absolute temperature in degrees Kelvin, K, and T_0 is the characteristic temperature. Characteristic temperature T_0 is an indicator of the laser sensitivity to temperature. High T_0 indicates good temperature tolerance. The characteristic temperature T_0, was estimated to be 153 K in the temperature range of 77K to 322K. \

4.4 References

[1] C.-H. Lee, J. Yoo, Y. J. Hong, J. Cho, Y.-J. Kim, S.-R. Jeon, J. H. Baek, and G.-C. Yi ”GaN/ In1−xGaxN/GaN/ZnO nanoarchitecture light emitting diode microarrays, ” Appl. Phys. Lett. **94**, 213101. (2009)

[2] Huang H W, Chu J T, Hsueh T H, Ou-Yang M C, Kuo H C and Wang S C ”Fabrication and photoluminescence of InGaN-based nanorods fabricated by plasma etching with nanoscale nickel metal islands,” J. Vac. Sci. Technol. B **24** 1909(2006)

[3] Justin C. Johnson, Heon-Jin Choi, Kelly P. Knutsen, Richard D., Schaller, Peidong Yang, and Richard J. Saykally, ” Single gallium nitride nanowire lasers, ” Nature, Materials **1**, 106 (2002)

[4] H. W. Huang, J. T. Chu, T. H. Hsueh, M. C. Ou-Yang, H. C. Kuo, and S. C. Wang “Fabrication and photoluminescence of InGaN-based nanorods fabricated by plasma etching with nanoscale nickel metal islands” J. Vac. Sci. Technol. B **24** 1909(2006)

[5] Ching-Lien Hsiao,a_ Li-Wei Tu,b_ Tung-Wei Chi,c_ and Min Chen “icro-Raman spectroscopy of a single freestanding GaN nanorod grown by molecular beam epitaxy” Appl. Phys. Lett., V. 90, 043102 (2007)

[6] S. Kako, T. Someya, and Y. Arakawa, “Observation of enhanced spontaneous emission coupling factor in nitride-based vertical-cavity surface-emitting laser,” Appl. Phys. Lett., vol. 80, pp. 722 (2002)

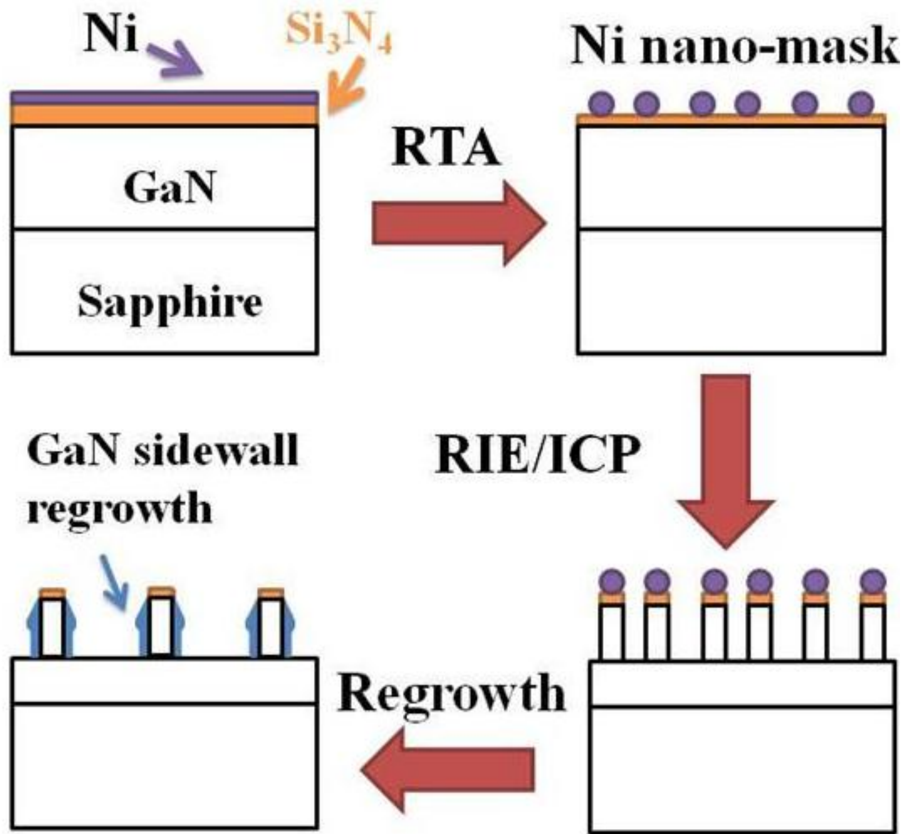

Fig. 4.1.1 Processing steps of nanopillars.

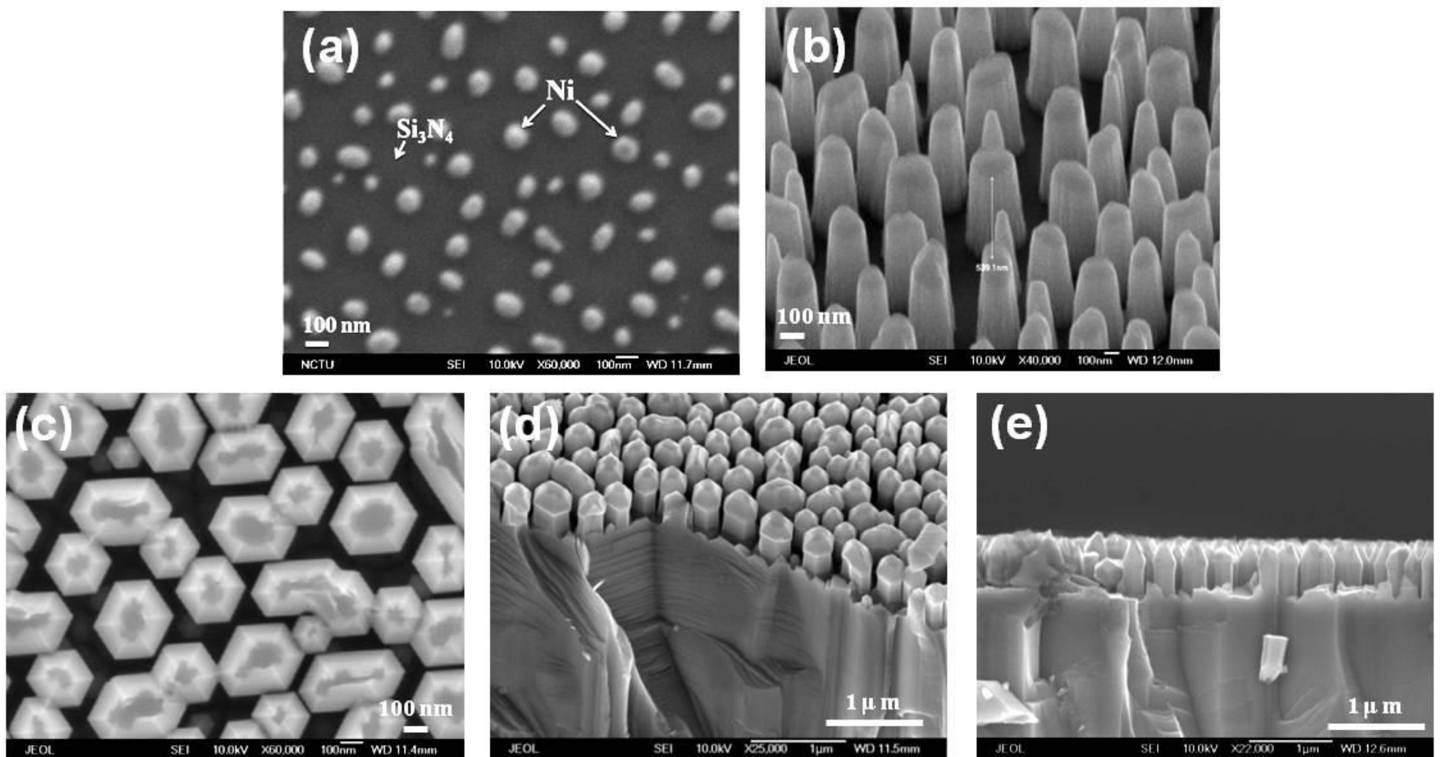

Fig.4.1.2 (a)Ni-mask on

Plane view (a), titled (b) and crossection (c) SEM images

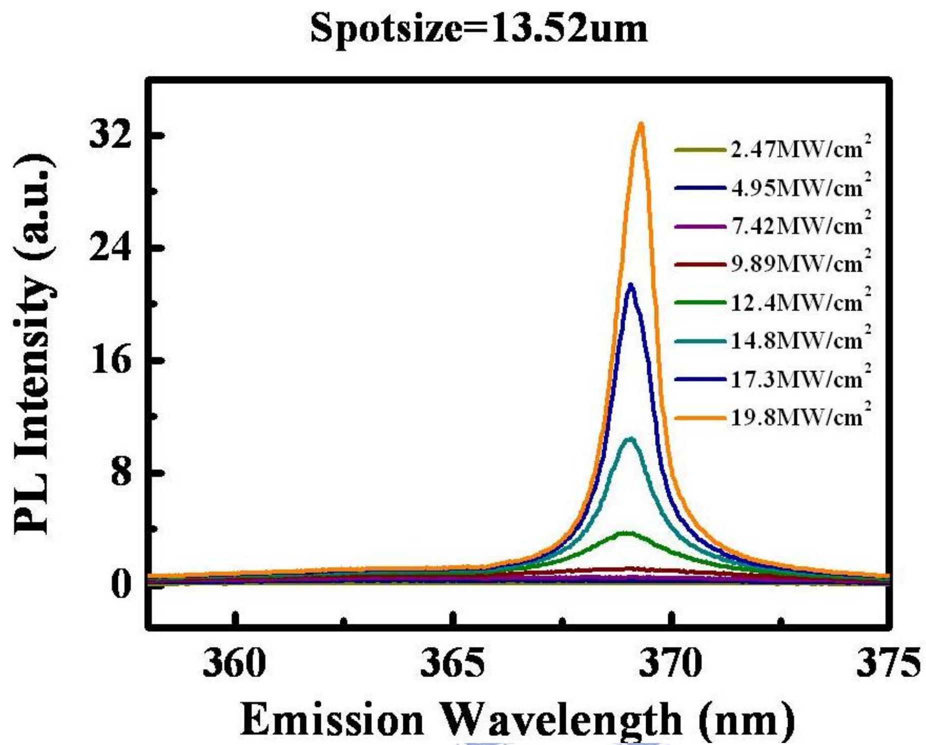

Fig 4.2.1.1 Power dependent PL spectrum of nanopillars with spotsize~13.5μm, and the stimulated emission wavelength at 369 nm

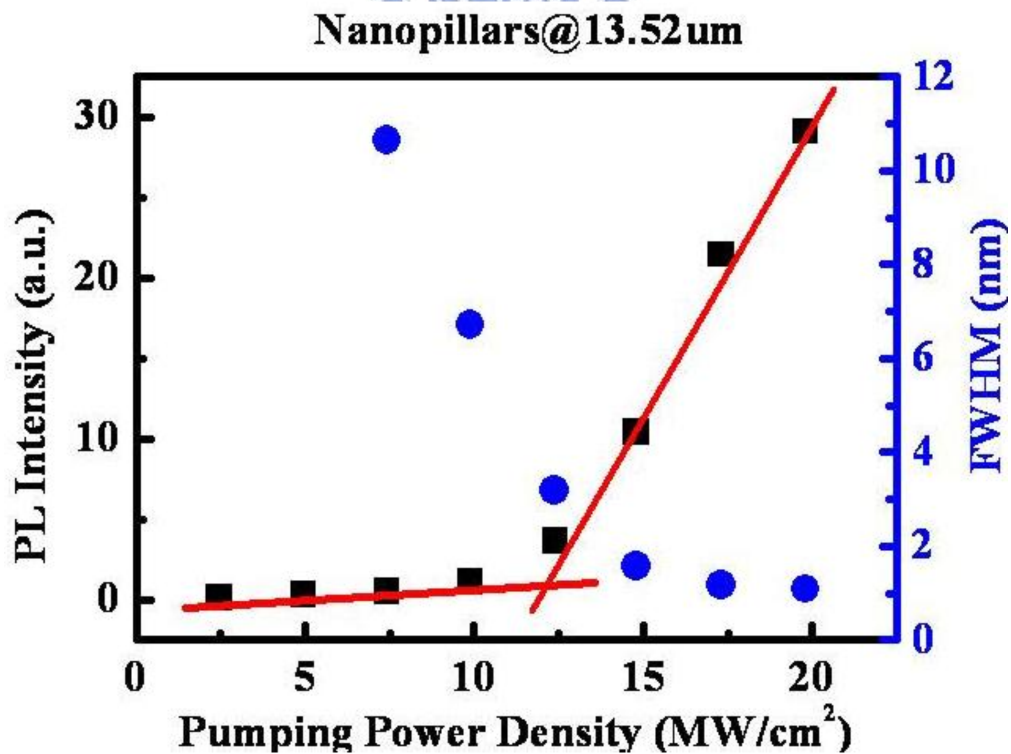

Fig 4.2.1.2 Light intensity and FWHM versus excitation power density of pillars.

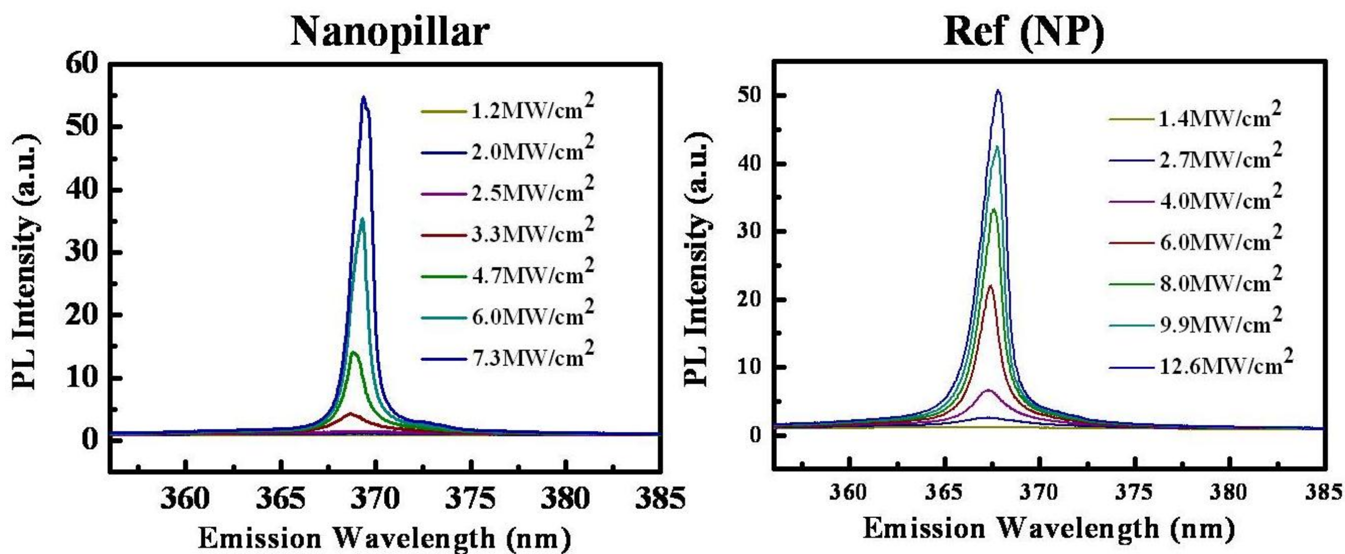

Fig 4.2.1.3 Power density dependent nanopillar and nanopillars without passivation (NP) with spotsize~ 37.1μm

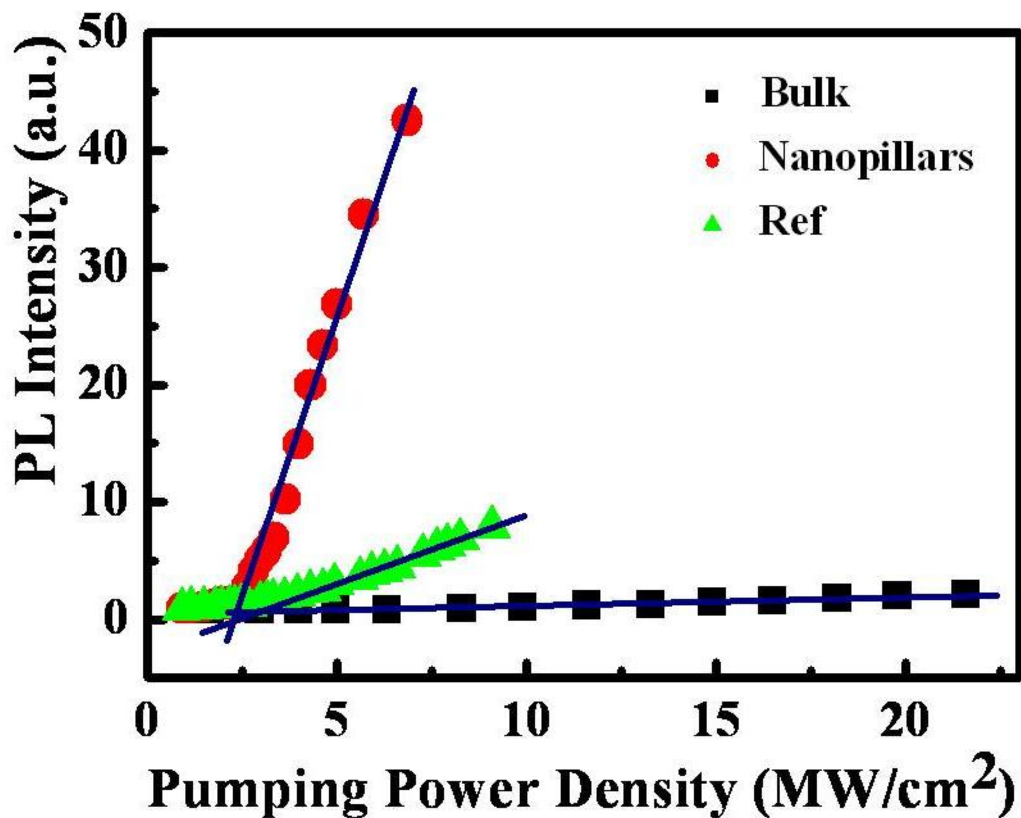

Fig 4.2.1.4 Light intensity and FWHM versus excitation power density of pillar,NP and bulk under 37.1μm laser beam.

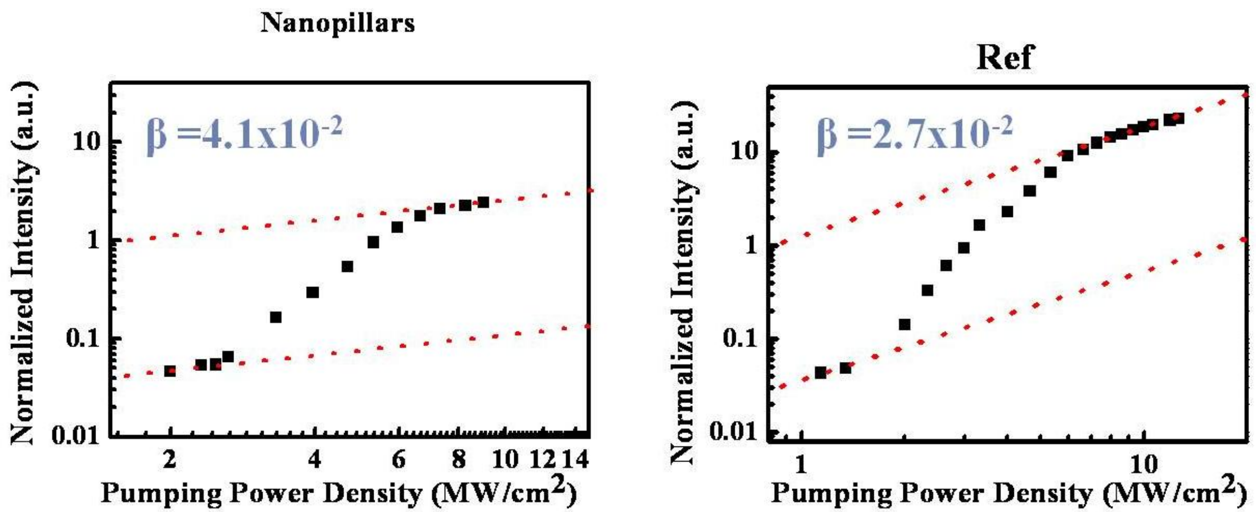

Fig 4.2.1.5 Input-output characteristic on logarithmic scales. Solid symbols are experimental data, and the line is theoretical fitting.

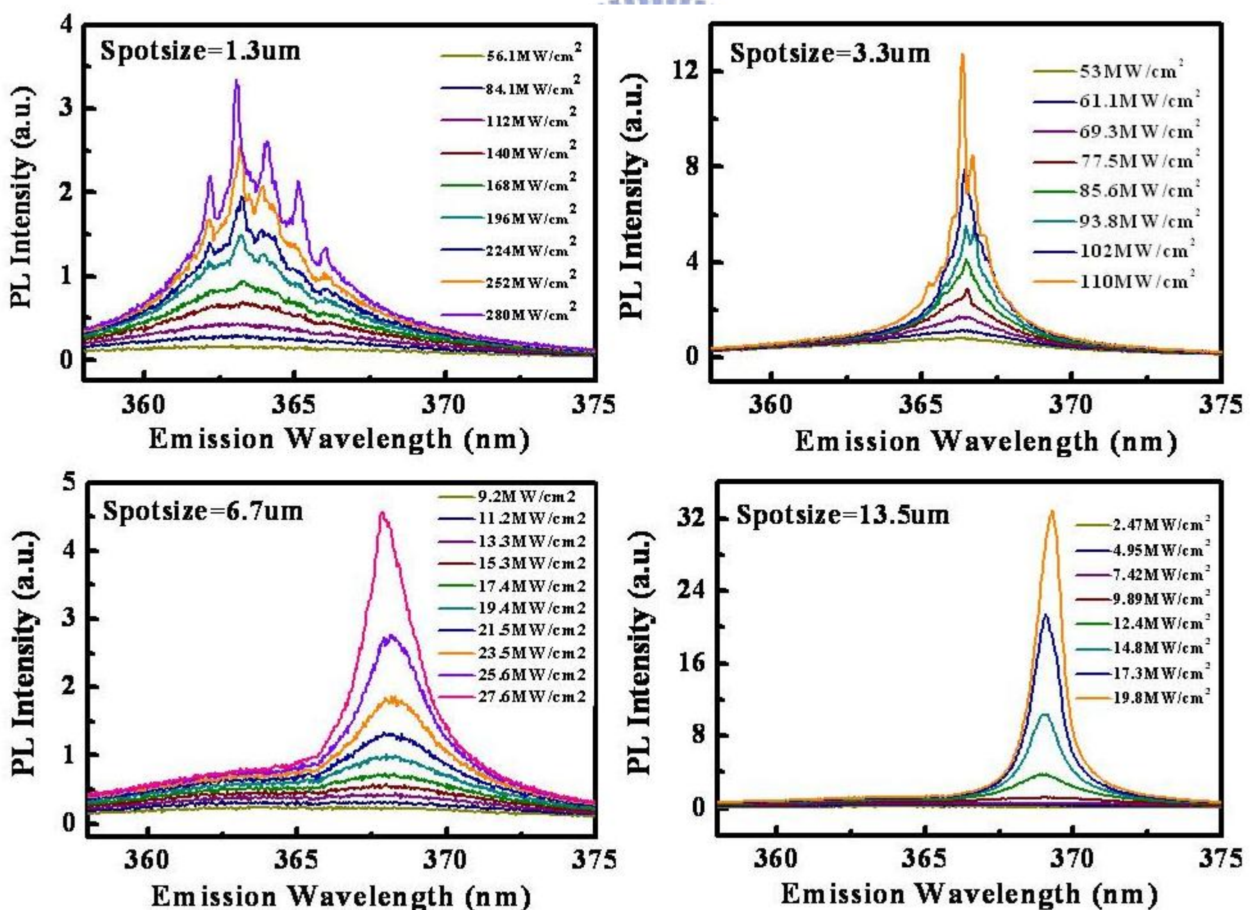

Fig 4.2.2.1 Power density dependent PL spectrum of pillar with various spotsize

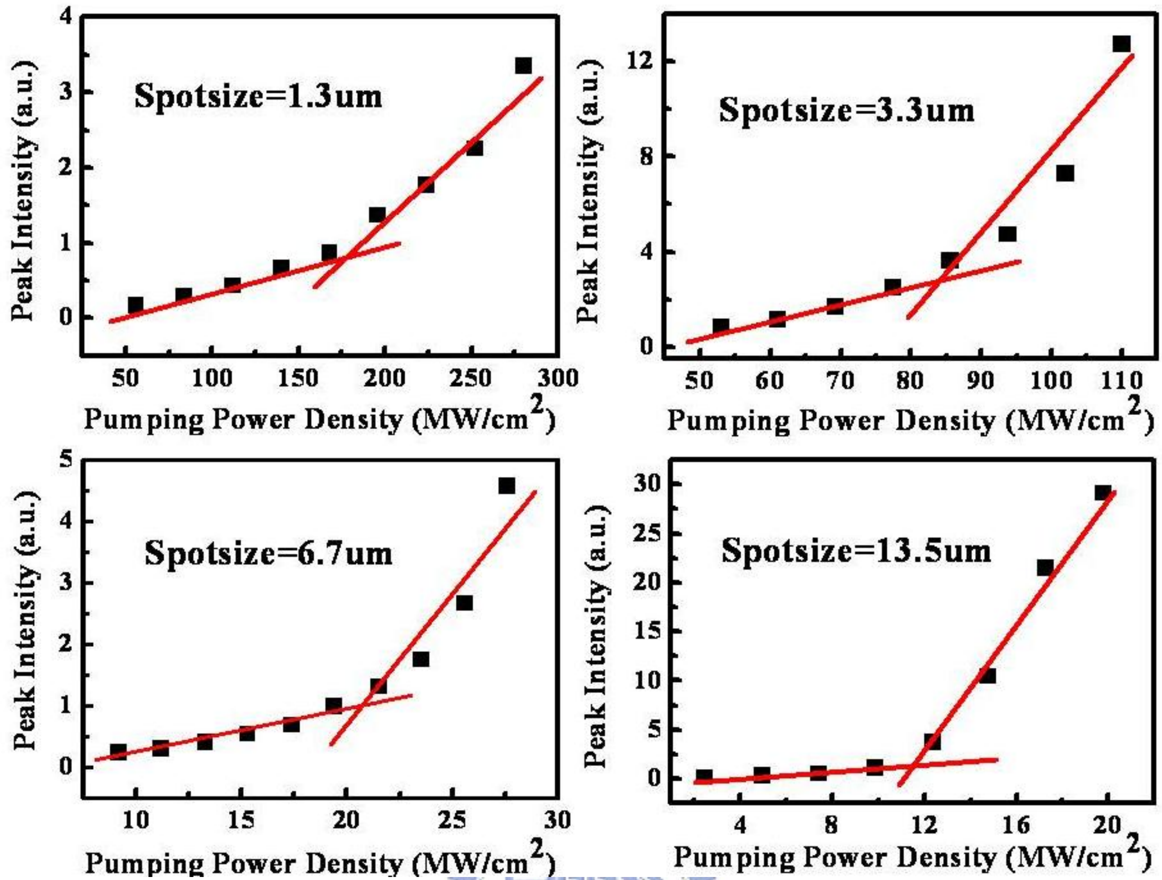

Fig 4.2.2.2 Threshold pumping power density of pillar with various spotsize

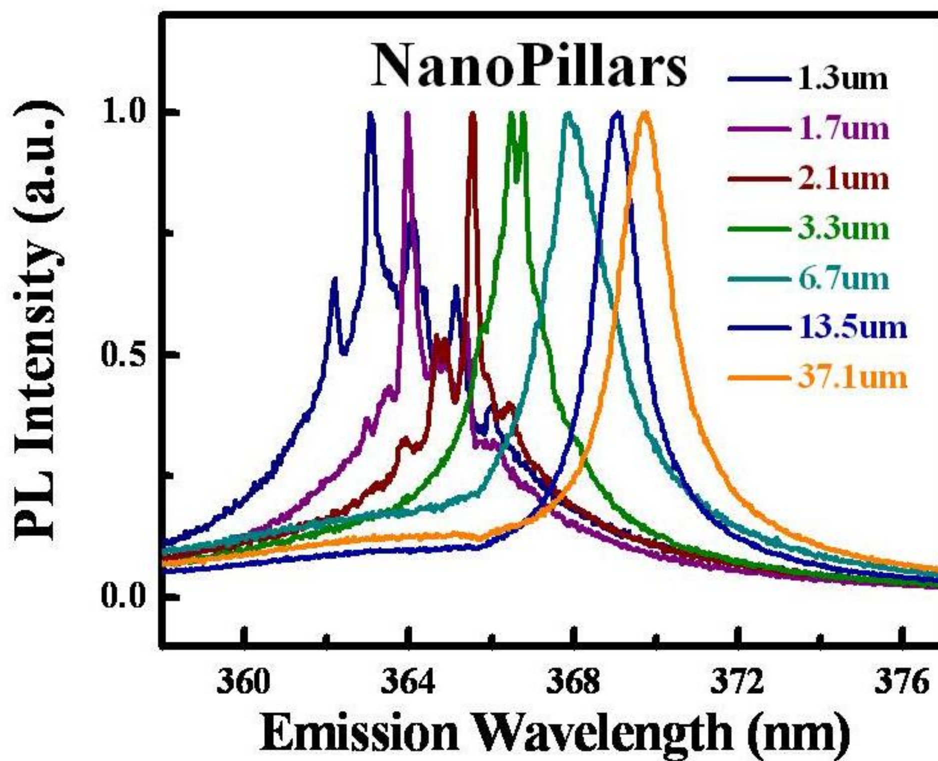

Fig 4.2.2.3 Comparison of various spotsize PL spectra

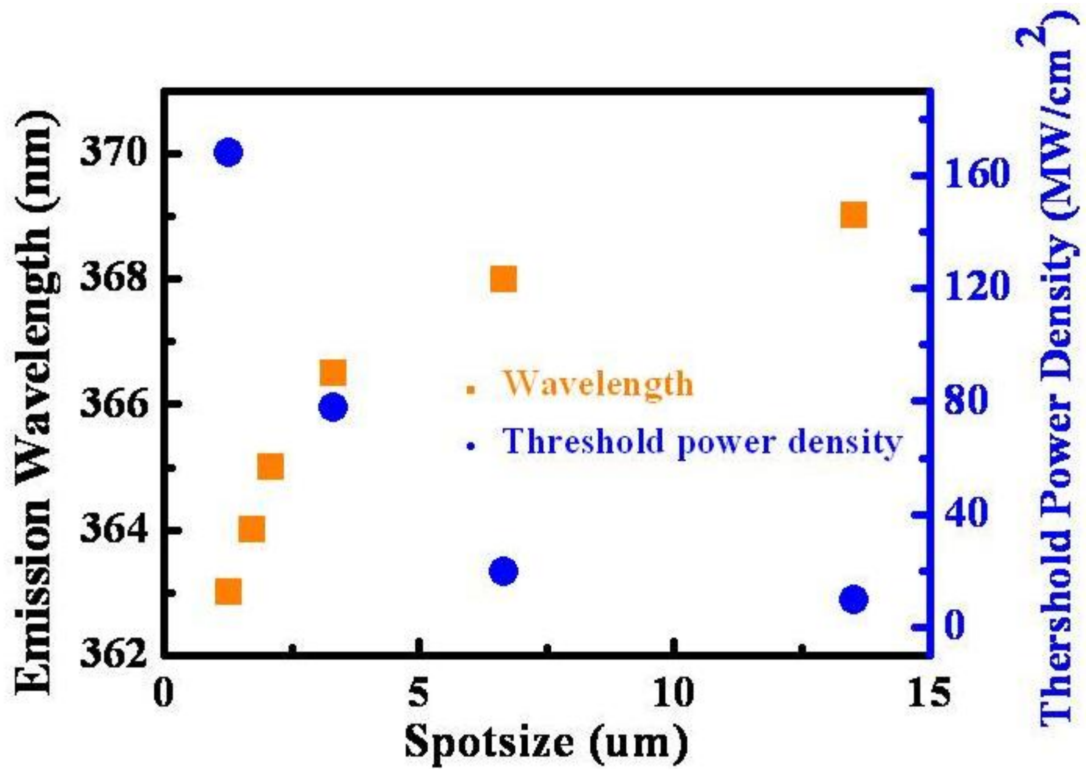

Fig 4.2.2.4 Emission wavelength and Threshold power density versus excitation spotsize of pillars.

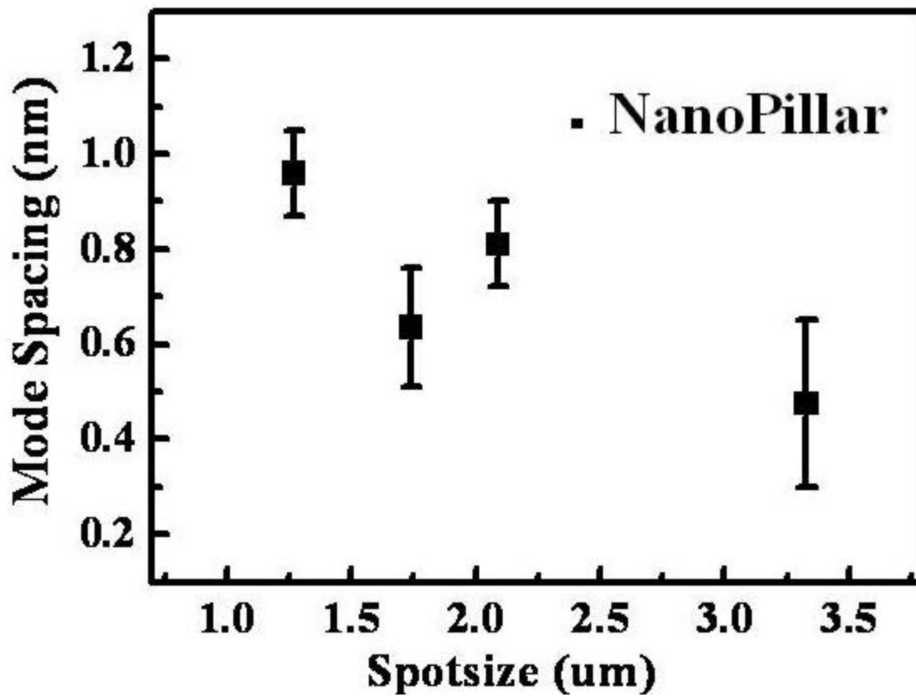

Fig 4.2.2.5 Mode spacingof pillar under various spotsize

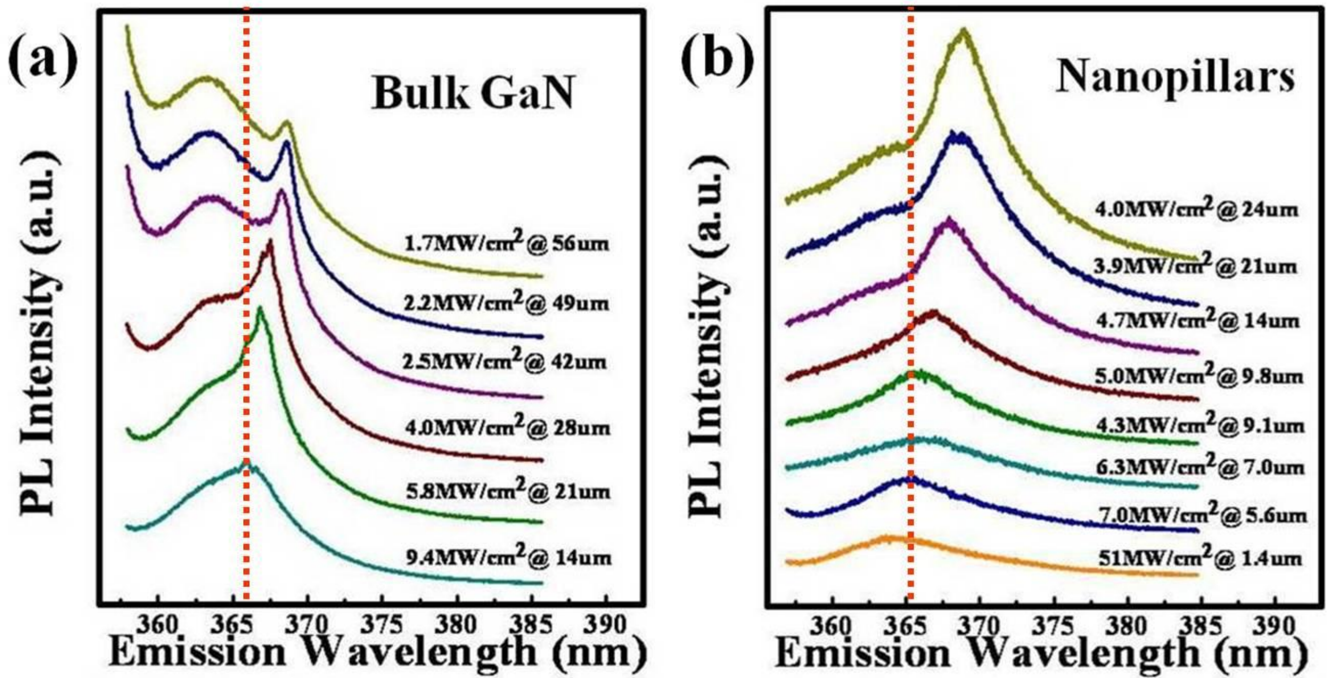

Fig 4.2.2.6 (a) GaN bulk gain spectra v.s spot size (b) Nanopillar gain spectra v.s spot size

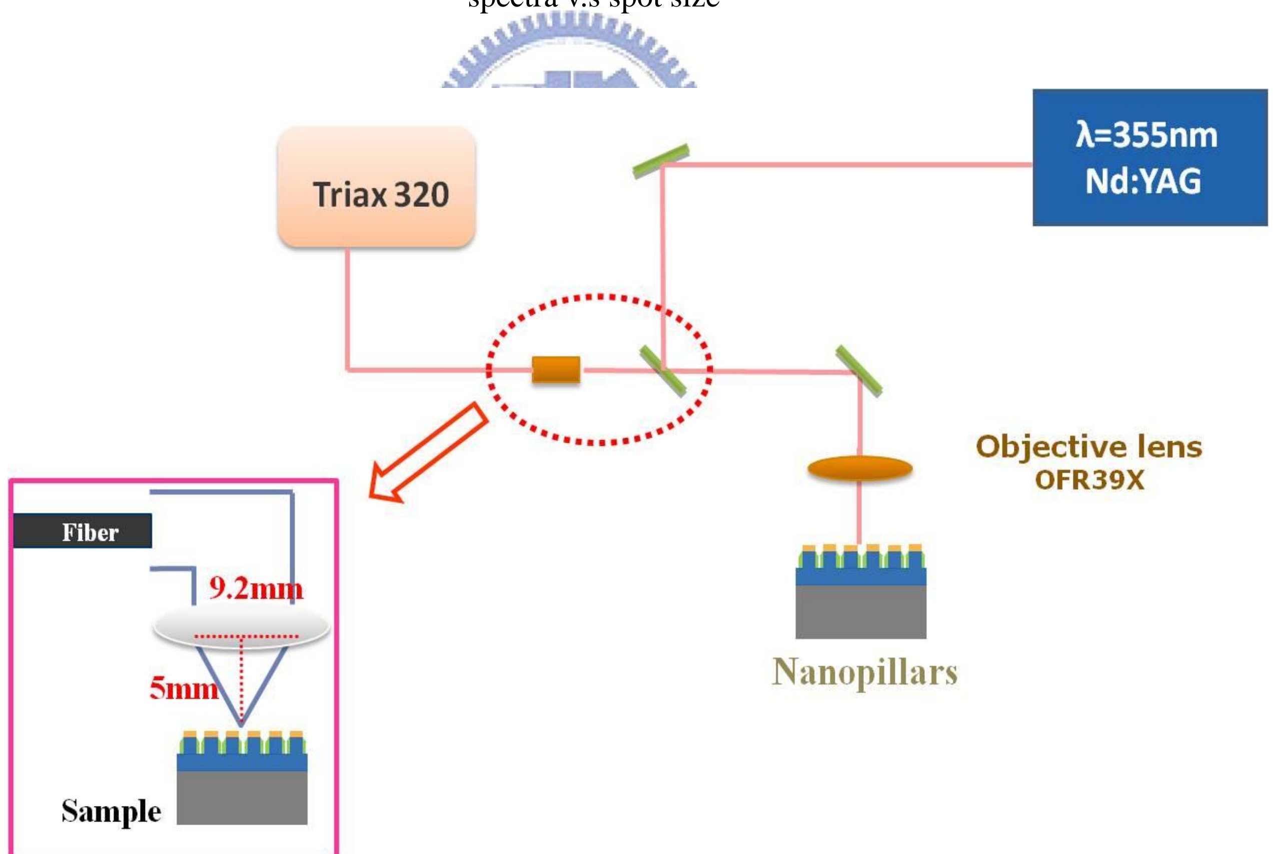

Fig 4.2.3.1 Angle-resolved μ-PL measurement system

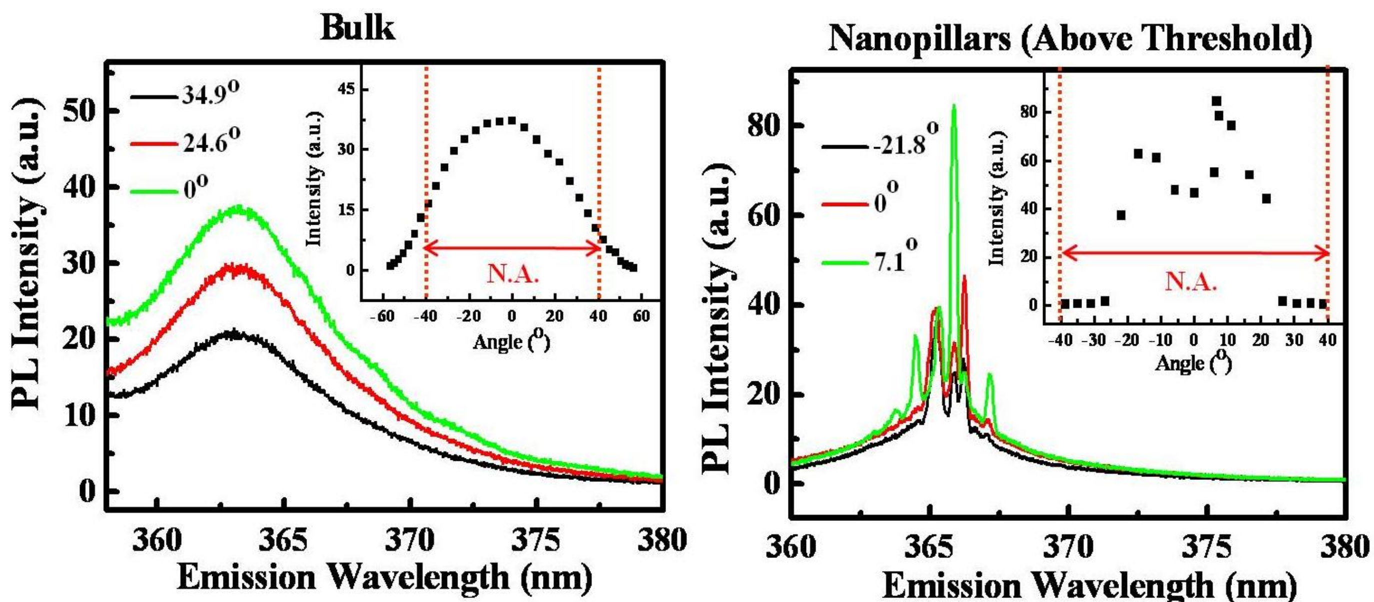

Fig 4.2.3.2 Angle-resolved μ-PL spectrum and intensity versus angle

(a)GaN bulk (b) Nanopillars

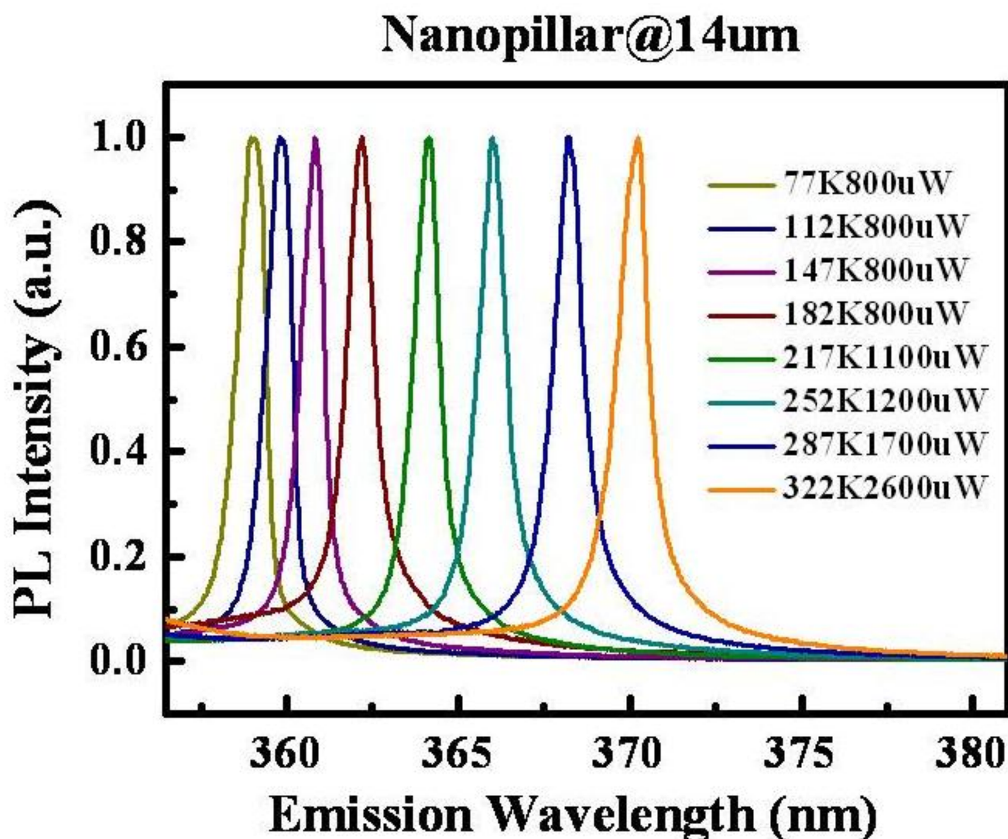

Fig 4.3.1 Temperature dependent PL spectrum of pillar

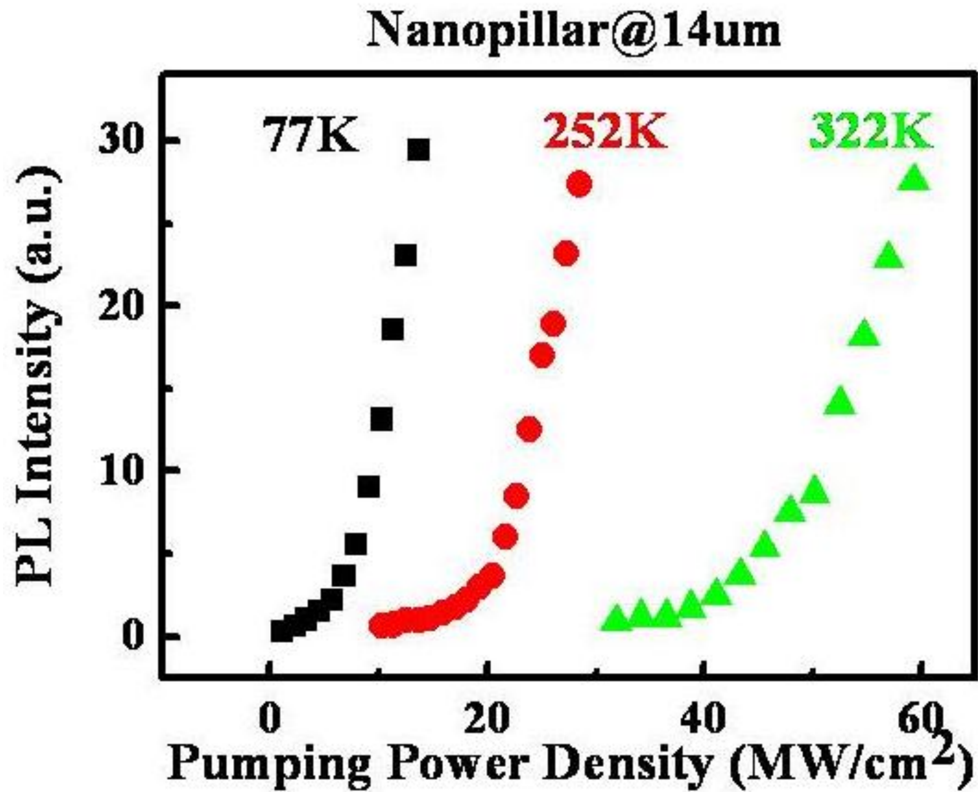

Fig 4.3.2 The emission intensity-excitation energy curve at 77K, 252K,and 322K

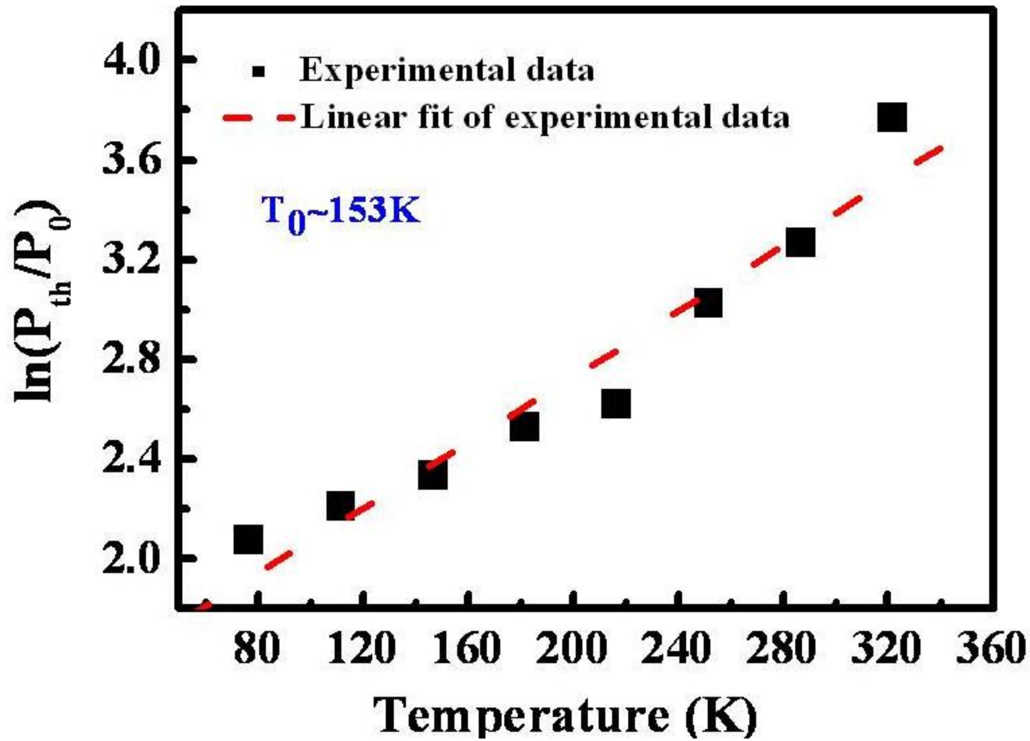

Fig 4.3.3 The temperature dependent threshold excitation power.

Chapter 5 Conclusion

In this thesis, we report the fabrication of nanopillars by self-assembled Ni nano-mask, etching, and MOCVD epitaxial regrowth, which results in hexagonal crystalline surfaces. We also analyzed the intensity data obtained by application of the traveling knife-edge method. Through use of simulated intensity data, diameters can be measured to an accuracy of 0.05%. The method yields good results when it is applied to Nd:YVO4 laser beam data.

Further, from our analysis, we investigated the different stimulated emission behavior of GaN nanopillars. Under laser spot size about 37.1μm, we repeat the measurement results from etched nanopillars, etched nanopillars without passivation (NP) and bulk samples included. It is fascinating to see such a stimulated emission from passivated nanopillars, the threshold excitation density is ~3.3MW/cm^2, and β value of nanopillars is about 2.1x10^{-1}. As excitaion spotsize increasing, the central position of lasing peak wavelength was gradual red-shift and the number of lasing multi-peak modes dreased. The threshold pumping density with spotsize from 1.27μm to 13.52μm (1.27μm,3.3μm,6.65μm,13.5μm) is 168MW/cm^2, 85.6MW/cm^2, 21.5MW/cm^2, 12.4 MW/cm^2 , respectively. We suggest that the peak shift effect of lasing peak was attributed to the

change of material gain spectrum under different pumping condition, not related to the pumping power intensity under change of spot size. The angle-resolved PL results show the degree of emission anlges corresponding to the normal direction (10˚, -15˚) respectively.

Moreover, it was observed that the increase in temperature (from 77K to 322K) leads to an increase in threshold excitation energy. It is due to the increase of non-radiated recombination and decrease of radiated recombination. The characteristic temperature T_0, was estimated to be 153 K in the temperature range of 77K to 322K.

Overall, according to the features of GaN-based nanopillars, the structure can be applied in the visible and UV laser and become the highly potential optoelectronic device in high power emitter applications.